NK Cell and Fibroblast-Mediated Regulation of Skin Squamous Cell Carcinoma Invasion by CLEC2A Is Compromised in Xeroderma Pigmentosum

Maria Gonçalves-Maia, Yannick Gache, Miguel Basante, Estelle Cosson, Emie Salavagione, Margot Muller, Françoise Bernerd, Marie Françoise Avril, Sébastien Schaub, Alain Sarasin, et al.

Section Tumor biology

NK cell and fibroblast-mediated regulation of skin squamous cell carcinoma invasion by CLEC2A is compromised in Xeroderma Pigmentosum

Maria Gonçalves-Maia[1], Yannick Gache[1,a], Miguel Basante[1,2,a], Estelle Cosson[3], Emie Salavagione[3], Margot Muller[1], Françoise Bernerd[4], Marie Françoise Avril[5], Sébastien Schaub[2], Alain Sarasin[6], Véronique M. Braud[3,b], Thierry Magnaldo[1,b]

[1]Université Côte d'Azur, INSERM, CNRS, Institute for Research on Cancer and Aging, Nice, U1081, UMR7284, Nice, France

[2]Université Côte d'Azur, CNRS, Inserm, Institut de Biologie Valrose, Nice, France

[3]Université Côte d'Azur, Centre National de la Recherche Scientifique, Institut de Pharmacologie Moléculaire et Cellulaire, UMR7275, Valbonne, Sophia Antipolis, France

[4]L'Oréal Research and Innovation, Aulnay-sous-Bois, France

[5]Assistance Publique-Hôpitaux de Paris, Department of Dermatology, Hospital Cochin, University Paris Descartes, Paris, France

[6]Univ. Paris-Sud, Institut Gustave Roussy, UMR8200, CNRS, F-94805, Villejuif, France

[a] Y.G. and M.B. contributed equally to this work

[b] T.M. and V.M.B. contributed equally to this work

ORCIDs

M. Goncalves-Maia: 0000-0002-9975-0180

Y. Gache: 0000-0002-5638-4854

M. Basante: 0000-0002-2396-6399

E. Cosson: 0000-0001-9482-1755

E. Salavagione: 0000-0003-0478-5872

M. Muller: 0000-0002-0371-7168

F. Bernerd: 0000-0001-5426-7948

M.F. Avril: 0000-0002-9112-8477

S. Schaub: 0000-0002-9624-3271

A. Sarasin: 0000-0002-2445-6016.

V.M. Braud: orcid.org/0000-0001-8213-3947

T. Magnaldo: orcid.org/0000-0001-9174-8599

Nice, Provence Alpes Côte d'Azur, France

Two corresponding Authors :

*Dr Thierry Magnaldo, DR, CNRS

Institute for Research on Cancer and Aging, Nice - INSERM U1081, CNRS UMR 7284, UNS

Faculté de Medecine

28, Avenue de Valombrose

06107 Nice Cedex 2 – France

Telephone: 0033493377670

Fax: 0033493377676

Email: Thierry.magnaldo@univ-cotedazur.fr

*Dr Véronique Braud, DR CNRS

Centre National de la Recherche Scientifique - CNRS/UNSA UMR 7275

Institut de Pharmacologie Moléculaire et Cellulaire

660 Route des Lucioles - 06560 Valbonne – France

Telephone: 33 4 93 95 77 71

Fax: 33 4 93 95 77 08

Email: braud@ipmc.cnrs.fr

Short title: CLEC2A regulates skin carcinoma invasion

Abbreviations

3D, three dimensional; CAFs, cancer-associated fibroblasts; CLEC2A, C-type lectin domain family 2 member A; KACL, keratinocyte-associated C-type lectin; NK, natural killer cells; PCA, principal component analysis; SCC, squamous cell carcinomas; TME, tumor microenvironment; XP, xeroderma pigmentosum

Keywords

Xeroderma Pigmentosum, skin, cancer-associated fibroblasts, natural killer, CLEC2A, NKp65

ABSTRACT

The ability of cancer cells to invade and disseminate can be affected by components of the surrounding microenvironment. To identify dermal components regulating the growth of epidermal carcinomas, we studied the xeroderma pigmentosum genetic disease that bears mutations in genes involved in nucleotide excision DNA repair. Xeroderma pigmentosum patients are more prone to develop cutaneous tumors compared to the general population and their dermal fibroblasts display features of dermal cancer-associated fibroblasts, promoting keratinocyte invasion. Here, we report that 3-dimensional dermal cultures of fibroblasts from healthy donors, but not from XP-C patients, express CLEC2A, the ligand of the activating Natural Killer cell receptor NKp65. A similar loss of CLEC2A was observed in sporadic dermal cancer-associated fibroblasts and upon culture of fibroblasts with cutaneous SCC-conditioned medium. Using an innovative 3-dimensional organotypic skin culture model that contain NK cells in addition to fibroblasts and SCC cells, we unveil a key role of CLEC2A that orchestrates a cross-talk between fibroblasts and NK cells leading to the control of SCC invasion. These findings indicate that CLEC2A-expressing dermal fibroblasts play a major role in skin immune surveillance.

INTRODUCTION

Skin cancer is the most frequent cancer worldwide and its prevalence has highly increased over the last thirty years (Bray et al., 2018). Patients suffering from xeroderma pigmentosum (XP), a rare genetic autosomal recessive disease caused by mutations in one of the seven XP genes involved in the nucleotide excision repair of DNA lesions after a UV stress, exhibit a very high propensity to develop cutaneous cancers (Kraemer et al., 1987, Lehmann et al., 2011). In these patients, non-melanoma skin cancers including basal cell carcinomas (BCC) and squamous cell carcinomas (SCC) are increased 10 000-fold and melanoma is increased 2000-fold compared to the general population (Bradford et al., 2011). Among the seven XP complementation groups, XP-C is the most frequent complementation group in Europe and USA (Keijzer et al., 1979, Kleijer et al., 2008). XP-C patients are highly susceptible to aggressive SCC skin cancers; however, mechanisms underlying this typology of XP-C skin cancer are not yet understood (Giglia et al., 1998).

Cancer progression depends on both mutations in cancer cells that favor their growth and spread, and the characteristics of the surrounding environment and its cellular components (Fidler, 2003). Within the tumor microenvironment (TME), fibroblasts represent a significant proportion of non-tumor cells, and they are converted into cancer-associated fibroblasts (CAFs) (Kalluri and Zeisberg, 2006). CAFs are irreversibly activated fibroblasts that change the architecture and composition of the TME, and are active stimulators of cancer growth and progression. CAFs are associated with poor survival in cancer patients. Immune cells also infiltrate tumors and can have anti- and pro-tumoral functions. Natural Killer (NK) cells have been shown to interact with cancer cells, both through direct contact and via chemokine and cytokine signaling. Their presence in the TME correlates with good prognosis in many types of cancer including skin cancers (Imai et al., 2000, Ishigami et al., 2000, Li et al., 1998).

Interestingly, fibroblasts and immune cells from XP patients exhibit specific phenotypes that resemble those of CAFs and immunocompromised immune cells, respectively (Bernerd et al., 2001, Mariani et al., 1992, Norris et al., 1988). XP-C fibroblasts, isolated from healthy non photo-exposed skin areas promote keratinocyte invasion in organotypic cultures (Bernerd et al., 2001). Like CAFs, they overexpress the hepatocyte growth factor (HGF) and Matrix Metalloproteinase 1 (MMP1) implicated in ECM remodeling (Bernerd et al., 2001, Cui et al., 2018, Frechet et al., 2008). Immune abnormalities have also been identified in XP patients. Several studies reported that NK cells from XP patients exhibit a deficiency in their lytic activity, suggesting that NK cell dysfunction may contribute to cancer progression in these patients (Mariani et al., 1992, Norris et al., 1988, Norris et al., 1990).

Based on these observations, we postulated that XP disease could be a good model to study development and progression of skin cancers. We therefore analyzed the gene expression profiles of three dimensional (3D)-dermal cultures of fibroblasts from healthy donors (WT) and XP-C patients. We identified C-type lectin domain family 2 member A (*CLEC2A*), the ligand of the activating NK cell receptor NKp65 (Spreu et al., 2007, Spreu et al., 2010) among the few differentially expressed genes. CLEC2A expression was lost in XP-C fibroblasts but also in CAFs. By developing a 3D organotypic skin culture model that contain NK cells, we unveil an important crosstalk between fibroblasts and NK cells that regulates SCC invasion.

RESULTS

CLEC2A differential gene expression in WT and XP-C fibroblasts from 3D-dermal cultures.

In an attempt to identify dermal components regulating the growth of skin cancers in XP-C patients, we examined the genome-wide expression profile of six primary independent fibroblast cell lines (3 WT, 3 XP-C) cultured in 3D-collagen matrices, using microarrays. Principal component analysis (PCA) showed that XP-C fibroblasts displayed a distinct transcriptomic profile and higher heterogeneity compared to WT fibroblasts (Figure1a). Twelve genes were found upregulated and ten downregulated in WT fibroblasts compared to XP-C fibroblasts (Figure1b and Supplementary Table S1 online). Among these genes, we identified *CLEC2A* as one of the genes that was the most significantly differentially expressed (Figure1b and Supplementary Table S1 online). Two *CLEC2A* transcripts variants, *CLEC2A1* and *CLEC2A*2 were found expressed in WT but not in XP-C fibroblasts (Figure1c). *CLEC2A*1 encodes for a cell surface molecule previously reported to be expressed in skin and by keratinocytes (Spreu et al., 2007). CLEC2A interacts with the activating receptor, NKp65, expressed by human NK cells (Spreu et al., 2010). The expression of CLEC2A in WT fibroblasts suggests a putative cross-talk between fibroblasts and NK cells in the skin of healthy individuals which may dysfunction in XP-C patients.

Selective expression of CLEC2A at the cell surface of cutaneous primary fibroblasts from healthy individuals.

To further document CLEC2A mRNA and protein expression, we analyzed a panel of WT and XP-C fibroblasts that we isolated from healthy and XP-C skin biopsies, using a previously published protocol (Otto et al., 1999). We confirmed the nature and purity of the primary fibroblasts which expressed CD90 (Supplementary FigureS1a online). Using a set of primers

that detects *CLEC2A1* together with *CLEC2A2* transcript variants, we identified *CLEC2A* transcripts in WT fibroblasts and not in XP-C fibroblasts (Figure2a). CLEC2A cell surface expression was also detected by flow cytometry on a large proportion of WT fibroblasts and not on XP-C fibroblasts (Figure2b and c). In addition, with primers specific for each transcript variant (Supplementary FigureS1b online), we detected *CLEC2A1* and *CLEC2A2* mRNA in WT fibroblasts and in CLEC2A-expressing cell line U937 (Spreu et al., 2007) but not in XP-C fibroblasts. Imaging flow cytometry revealed that CLEC2A was predominantly expressed at the cell surface in WT fibroblasts (Supplementary FigureS1c online). As CLEC2A1 isoform was reported to be expressed at the plasma membrane while CLEC2A2 remained intracellular (Spreu et al., 2007), the observed CLEC2A at the cell surface is likely to relate to the accumulation of *CLEC2A1* rather than *CLEC2A2* variants. The puzzling lack of CLEC2A expression in XP-C fibroblasts led us to investigate the origin of this defect. Mutations in the *XPC* gene are mostly deleterious (Stary and Sarasin, 2002). Beyond nucleotide excision repair, XPC has been suggested to have a role in the regulation of transcription and in the reprogramming of induced pluripotent stem-cells (Fong et al., 2011, Le May et al., 2010). Therefore, we considered the possibility that the XPC protein was directly regulating CLEC2A expression. To test this hypothesis, we efficiently restored wild type-XPC expression in XP-C fibroblasts by retroviral transduction of a cassette containing a normal version of *XPC* cDNA (Supplementary FigureS2a online). We confirmed that transduced XP-C fibroblasts were able to perform efficient DNA repair after UV radiation, using the measurement of unscheduled DNA synthesis (UDS) by incorporation of 5-ethynyl-2′-deoxyuridine (EdU) labeled nucleotides into the newly DNA patches that are synthetized upon DNA repair (Supplementary FigureS2b online). Under these conditions, however, expression of *CLEC2A* was not restored in XP-C reverted fibroblasts (Supplementary FigureS2c online). Altogether, these data

highlight a default of CLEC2A expression in XP-C patients that is not directly reverted after XPC re-expression.

Downregulation of CLEC2A expression within SCC tumor microenvironment.

The evidence that XP-C fibroblasts may behave like CAFs, enhancing epidermal invasion, even in absence of cancerous cells (Bernerd et al., 2001) prompted us to look into the expression of CLEC2A in human dermal CAFs. To assess whether CLEC2A could be modulated in SCC microenvironment, we isolated two different dermal CAF cell lines from DNA repair-proficient human skin SCCs. Both cell lines positively expressed α-SMA, consistent with a *bona fide* CAF phenotype (Figure3a). Contrary to control WT fibroblasts, CLEC2A transcripts and protein could not be detected in these two dermal CAFs cell lines (Figure3b and c). Similarly, we did not detect CLEC2A transcripts and proteins in BCC-associated fibroblasts, highlighting that a similar defect applies to SCC and BCC-associated fibroblasts (Supplementary FigureS3 online). These data suggested that the expression of CLEC2A in skin fibroblasts may be downregulated during tumor development, upon transformation of normal fibroblasts into CAFs. To test this hypothesis, we generated conditioned-medium from the culture of the SSC12 tumor cell line that is able to convert WT fibroblasts into CAFs *in vitro*, as shown by the induction of α-SMA on SCC12-conditioned medium (SSC12_CM)-treated WT fibroblasts (Figure4a). We then studied the impact of factors secreted by SCC12 tumor cell line on CLEC2A expression. After 5 days of incubation with SCC12_CM, the expression of CLEC2A in WT fibroblasts was found downregulated both at mRNA and protein levels (Figure4b and c). By contrast, no significant modulation in CLEC2A expression was seen after incubation of WT fibroblasts with conditioned-media from another WT fibroblast and WT keratinocytes (Supplementary FigureS4a and b online). TGF-β is one major driver of the transition of WT fibroblasts into CAFs (Albrengues et al., 2014, Desmouliere et al., 1993). We checked the possible role of TGF-β in the modulation of

CLEC2A. Supplementation of the culture medium with TGF-β did not decrease *CLEC2A* mRNA transcripts while it induced α-SMA expression (Supplementary FigureS4c and d online). Moreover, neutralizing TGF-β in SCC12_CM by addition of an anti-TGF-β did not block CLEC2A downregulation triggered by SCC12_CM (Supplementary FigureS4c online). We concluded that TGF-β was not responsible for the downregulation of CLEC2A expression in WT fibroblasts during their transition to CAFs in the TME. We then screened a large panel of cytokines and we identified three inflammatory cytokines, IL-1α, IL-1β and TNF-α that could induce a significant downregulation of CLEC2A cell surface expression when supplemented in the culture medium (Figure4d). To assess whether these three cytokines are implicated in the downregulation of CLEC2A by the SCC12_CM, we depleted this CM of IL-1α, IL-1β and TNF-α. While CLEC2A cell surface expression on WT fibroblasts was downregulated by the SCC12-CM or the control SCC12-CM treated with Protein-G-sepharose beads, CLEC2A was maintained on a significant proportion of WT fibroblasts cultured in the presence of SCC12-CM depleted of the three cytokines (Figure4e). Collectively, our findings indicate that the tumor microenvironment and specifically IL-1α, IL-1β and TNF-α modulate CLEC2A expression on fibroblasts.

Expression of CLEC2A and NKp65 in healthy and XP-C skin.

CLEC2A binds with high affinity the activating receptor NKp65 encoded by *KLRF2* gene that has been mostly described in the NK92 human NK cell line and has not been detected in resting NK cells (Bauer et al., 2015, Li et al., 2013, Spreu et al., 2010). In this study, we show that allogeneic stimulation of NK cells induces *KLRF2* transcripts. We isolated NK cells from peripheral blood of healthy individuals and expanded them upon allogeneic stimulation. *KLRF2* transcripts were detected in these NK cells by quantitative RT-PCR, at a higher level than in U937 cells used as positive control. No *KLRF2* transcripts were detected in tonsils, SCC12 and WT fibroblasts (Figure5a). Detection of transcripts of both *CLEC2A* and *KLRF2*

has been reported almost exclusively in skin and some *KLRF2* transcripts were also detected in tonsil, duodenum, lymph node and spleen at much lower level (Supplementary FigureS5a online and b). This suggests that expression of NKp65 may be highly regulated. The lack of available anti-NKp65 antibody has so far hampered the full characterization of its protein expression profile. To circumvent this, we set up *in situ* hybridization using the RNAscope® technology and newly designed probes to visualize *CLEC2A* and *KLRF2* transcripts in skin (Figure5b). We report here that *KLRF2* transcripts were exclusively detected in the dermis of healthy skin and not in XP-C skin. *KLRF2* transcripts were rare events, consistent with the reported low frequency of NK cells in human healthy skin (Antiga et al., 2017, Ebert et al., 2006) and with the lack of *KLRF2* transcripts in resting NK cells. By contrast, *CLEC2A* transcripts were found both in the dermis and the epidermis and they were more abundant in the epidermis, in agreement with the reported expression in keratinocytes (Spreu et al., 2010). We detected much lower levels of *CLEC2A* transcripts in XP-C skin and mostly in the epidermis, in agreement with the observed lack of CLEC2A expression in XP-C fibroblasts (Figure1, 2 and 5b). Interestingly, we were able to visualize co-localization of the two probes in the dermis of healthy skin, consistent with skin-resident NK cells expressing NKp65 interacting with CLEC2A-expressing fibroblasts.

CLEC2A regulates SCC invasion through a cross-talk between fibroblasts and NK cells.

To determine whether the loss of CLEC2A in XP-C fibroblasts and CAFs has an impact on cancer progression, we developed an innovative 3D-NK immunocompetent organotypic culture model to measure SCC invasion in the presence or absence of NK cells (Figure6a). We used NK cells from healthy individuals that were expanded upon allogeneic stimulation and thus possessed *KLRF2* transcripts (Figure5a). These NK cells expressed several activating receptors including CD16, NKG2D, and NKp46 (Supplementary FigureS6a online) and they killed SCC12 and not the WT and XP-C fibroblasts that we added in the 3D-NK-

immunocompetent organotypic skin cultures (Figure6b) (Fassy et al., 2017a, Fassy et al., 2017b). Interestingly, SCC12 cells, like WT and XP-C fibroblasts, express MHC-I molecules (Supplementary FigureS6b online). Killing of SCC12 may therefore results from abundant expression of ligands of activating NK receptors, excluding NKp65 as SCC12 do not express CLEC2A (Supplementary FigureS6c online). To quantify invasion rates, we developed the Epidepth software, and we were thus able to measure SCC12 invasion rates in different 3D-NK immunocompetent organotypic skin culture conditions (Figure6c and d; Supplementary FigureS7 online). Our results showed that the presence of NK cells significantly reduced the levels of SCC12 invasion in a 3D-NK immunocompetent organotypic skin culture containing CLEC2A-expressing WT fibroblasts. In sharp contrast, NK cells failed to limit SCC12 invasion rates in a 3D-NK immunocompetent organotypic culture containing CLEC2A-deficient XP-C fibroblasts and CAFs (Figure6c and d; Supplementary FigureS7 online). When we added the anti-CLEC2A blocking antibody OMA1 to the 3D-NK immunocompetent organotypic skin cultures containing WT fibroblasts, SCC12 invasion was restored to levels similar to those of the condition without NK cells (Figure6c and d; Supplementary FigureS7 online). This was not the case when the isotype Ig was added as a control. These results reveal a direct and positive impact of CLEC2A expression by WT fibroblasts in controlling SCC12 invasion via the activation of NK cells. Altogether, these results indicate that the cross-talk between fibroblasts and NK cells via CLEC2A interaction with NKp65 plays a role in the regulation of SCC invasion and progression.

DISCUSSION

Our findings uncover a key interaction between dermal fibroblasts and NK cells through CLEC2A/NKp65 interaction that could participate to immune surveillance of the skin.

The data described here show that CLEC2A is expressed in skin primary dermal fibroblasts of healthy individuals but is absent in skin primary dermal fibroblasts of cancer-prone XP-C patients and in CAFs. Expression of CLEC2A in dermal fibroblasts is further supported by the detection of *CLEC2A* transcripts in the dermis of healthy skin using *in situ* hybridization. These findings are consistent with the Human Protein Atlas database reporting a specific expression in the skin and in a foreskin cell line of human dermal fibroblast immortalized by ectopic expression of telomerase (https://www.proteinatlas.org/). Expression of CLEC2A was also recently reported in a single-cell transcriptional profiling of human dermal fibroblasts and was found to be differentially expressed between papillary and reticular dermis (Philippeos et al., 2018). Besides expression in fibroblasts, *in situ* hybridization revealed abundant *CLEC2A* transcripts in keratinocytes at all stages of differentiation in the epidermis. Thus, our data complement previous reports that described expression of CLEC2A in keratinocytes and restricted to skin and bone marrow (Spreu et al., 2007, Spreu et al., 2010). Consistent with these findings, recent single cell RNA sequencing profiles of epidermal keratinocytes identified low level of *CLEC2A* transcripts, more specifically in the spinous and basal layers (Cheng et al., 2018).

Fibroblasts are prominent cells in the dermis and they become irreversibly activated and convert into CAFs in the surroundings of tumors. In organotypic skin cultures, XP-C fibroblasts contribute to numerous proliferative epidermal invasions that are reminiscent of early steps of neoplasia (Bernerd et al., 2001). The absence of CLEC2A expression in XP-C fibroblasts led us to analyze whether CAFs could share this feature. The finding that CAFs also lack expression of CLEC2A suggests that loss of CLEC2A could be part of the transition process that WT fibroblasts undergo to become CAFs. As XPC has been suggested to have a role in the regulation of transcription (Fong et al., 2011, Le May et al., 2010), we reasoned that lack of XPC could directly lead to loss of CLEC2A but our results demonstrate that the absence of

CLEC2A expression in XP-C fibroblasts is not directly (nor immediately) dependent on the expression of a DNA repair-active XPC protein. Rather, soluble factors secreted by SCC were found to downregulate CLEC2A. The prime candidate TGF-β could not modulate CLEC2A expression on fibroblasts *in vitro* while TNF-α, IL-1α and IL-1β downregulated CLEC2A. These inflammatory cytokines are highly abundant in the tumor microenvironment and can thus contribute to tumor escape from NK cell-mediated cytotoxicity. Whether they also contribute to the loss of CLEC2A by XP-C fibroblasts still needs to be determined. Alternatively, because epigenetic modifications are often responsible for CAFs transformation and activation, more frequently than somatic mutations (Campbell et al., 2011, Jiang et al., 2008, Qiu et al., 2008) and because XP proteins have been involved in epigenetic control, notably DNA methylation (Ho et al., 2017), it remains to determine whether the modulation of CLEC2A in XP-C patients could be linked to such epigenetic control.

The selective expression of CLEC2A and NKp65 in the skin is a unique feature in support of a role of CLEC2A/NKp65 interaction in immune surveillance of the skin. Cross-talk between fibroblasts and NK cells is poorly documented but may contribute to SCC progression. Reports show that CAFs can exert immunosuppressive functions, such as impairment of immune cell recruitment or decrease of their cytotoxic potential (Li et al., 2012, Zelenay et al., 2015, Ziani et al., 2017). To address such questions, we developed a 3D-NK immunocompetent organotypic skin culture model in which we added NK cells and blocking anti-CLEC2A antibodies. We show that CLEC2A plays a central anti-tumoral role in skin, as NK cells are only able to hamper SCC invasion when CLEC2A-expressing fibroblasts are included in the cultures. This finding highlights a crucial role of the cross-talk between fibroblasts and NK cells. We propose that CLEC2A could facilitate the elimination of cancer cells by NK cells at early tumorigenesis stages, when fibroblasts have not yet shifted to a CAF phenotype and have not yet lost CLEC2A expression. In XP-C patients and during tumor progression, the loss of

CLEC2A may therefore contribute to immune dysfunctions leading to the observed increased incidence of aggressive SCC in these individuals. Restoring such immune surveillance might strengthen treatments of skin cancers.

MATERIALS AND METHODS

Tissues and cells. Normal human skins were collected from mammary or abdominal plastic resection surgery. XP skin biopsies were collected from non sun-exposed and normally pigmented sites. Skin SCC biopsies were collected from patients undergoing surgical excision. All samples were obtained with the patient's or parents' written informed consent according to the Declaration of Helsinki under local French ethic committee (CCPPRB: CSET935) or under institutional review board (Hôpital Pasteur, Centre Hospitalier Universitaire de Nice, France) approval. Human fibroblasts from healthy, XP-C or cancer patients were obtained and cultured as described (Otto et al., 1999). Cells are described in detail in supplementary Table S2 on line. NK cell lines were generated from human blood purchased from the Etablissement Français du Sang (Marseille, France), as previously described (Fassy et al., 2017b). SCC12 cells were a gift from James Reinwald (Brigham and Woman's Hospital, Harvard School of Medicine). Tonsil cells were obtained from discarded benign tonsils after informed consent from patients undergoing routine tonsillectomies at the Lenval Hospital, Nice. U937 (CRL-1593.2) and K562 (CCL-243) were purchased from ATCC.

3D-dermal and 3D-NK immunocompetent organotypic skin cultures. For transcriptomic analysis, fibroblasts (1×10^6) were cultured in a tridimensional type I collagen matrix at a concentration of $2{,}5 \times 10^5$ cells/mL for 4 days. After that, the matrix was cultured 7 days in immersion and then 7 days at the air-liquid interface as described in (Bernerd et al., 2001, Valin et al., 2009). For 3D immunocompetent models, fibroblasts (5×10^5) were cultured for 24 h in

a tridimensional type I collagen matrix at a concentration of 2,5 x 10^5 cells/mL. Then, SCC12 cells (2,5 x 10^5) were dissociated and seeded on the top of the matrix. The organotypic constructs were cultured 48 h in immersion and then 5 days at air-liquid interface. To incorporate NK cells into the model, we cultured NK cells (5 x 10^5) in a type I collagen matrix at 5 x 10^5 cell/mL for 24 h in a transwell insert (Corning) and then we added the fibroblasts-SCC12 construct on the top at air-liquid interface, allowing NK cells to migrate up to "dermal" compartment for 48 h (Figure6a).

***In situ* Hybridization:** Skin sections were dual labelled for the mRNA of *CLEC2A (ACD* #81942) and KLRF2 (ACD # 819431-C2), using RNAScope ® 2.5 Duplex Detection Kit following manufacturer's protocol. Images were acquired using a Leica DMD108 microscope.

DATA AVAILABILITY

The authors confirm that the data supporting findings of this study are available in the article and its Supplementary Materials. The data reported in this paper have been deposited in the Gene Ex-pression Omnibus (GEO) database, https://www.ncbi.nlm.nih.gov/geo (accession nos. GSE133084).

CONFLICT OF INTEREST

The authors state no conflict of interest.

ACKNOWLEDGEMENTS

We thank Dr. O. Camuzard (Hôpital Pasteur, Centre Hospitalier Universitaire de Nice, France) for providing biopsies for CAF skin extractions, and F. Tessier and A. Popa (supported by Canceropôle PACA) for bioinformatics assistance. We thank Professor Alexander Steinle for kindly providing the anti-CLEC2A antibody OMA1. The authors acknowledge the IPCM's

Genomic and Imaging/Cytometry core facilities and IRCAN's Cytometry (Cytomed), Microscopy (PICMI) Histology and Genomic core facilities.

This work was supported by the French Government (National Research Agency, ANR; CNRS; INSERM) through the 'Investments for the Future' LABEX SIGNALIFE: program reference # ANR-11-LABX-0028-01; UCA (Université Côte d'Azur) and Association René Tourraine. MGM was supported by the Fondation de l'Avenir (PhD fellowship 2015) and LABEX SIGNALIFE; TM was supported by the Fondation ARC (SFI201212055859), the Fondation de l'Avenir, Société Française de Dermatologie, and The Institut National du Cancer. VMB was supported by Centre National de la Recherche Scientifique, Cancéropole PACA, Région Provence-Alpes-Côte d'Azur, Institut National du Cancer and Fondation ARC pour la recherche sur le Cancer.

AUTHOR CONTRIBUTIONS

Conceptualization: MGM, VMB, TM; Data curation: MGM; Formal Analysis: MGM, YG, MB, VMB, TM; Funding Acquisition: FB, VMB, TM; Investigation: MGM, YG, MB, EC, ES, MM; Methodology: MGM, SS; Project Administration: MGM, VMB, TM; Resources: FB, MFA, AS ; Software : SS ; Supervision: VMB, TM; Validation: MGM, VMB, TM ; Visualization: MGM, VMB, TM ; Writing – Original Draft Preparation: MGM, VMB, TM.

REFERENCES

Albrengues J, Bourget I, Pons C, Butet V, Hofman P, Tartare-Deckert S, et al. LIF mediates proinvasive activation of stromal fibroblasts in cancer. Cell reports 2014;7:1664-78.

Antiga E, Maglie R, Volpi W, Bianchi B, Berti E, Marzano AV, et al. T helper type 1-related molecules as well as interleukin-15 are hyperexpressed in the skin lesions of patients with pyoderma gangrenosum. Clinical and experimental immunology 2017;189:383-91.

Bauer B, Spreu J, Rohe C, Vogler I, Steinle A. Key residues at the membrane-distal surface of KACL, but not glycosylation, determine the functional interaction of the keratinocyte-specific C-type lectin-like receptor KACL with its high-affinity receptor NKp65. Immunology 2015;145:114-23.

Bernerd F, Asselineau D, Vioux C, Chevallier-Lagente O, Bouadjar B, Sarasin A, et al. Clues to epidermal cancer proneness revealed by reconstruction of DNA repair-deficient xeroderma pigmentosum skin in vitro. Proceedings of the National Academy of Sciences of the United States of America 2001;98:7817-22.

Bradford PT, Goldstein AM, Tamura D, Khan SG, Ueda T, Boyle J, et al. Cancer and neurologic degeneration in xeroderma pigmentosum: long term follow-up characterises the role of DNA repair. J Med Genet 2011;48:168-76.

Bray F, Ferlay J, Soerjomataram I, Siegel RL, Torre LA, Jemal A. Global cancer statistics 2018: GLOBOCAN estimates of incidence and mortality worldwide for 36 cancers in 185 countries. CA: a cancer journal for clinicians 2018;68:394-424.

Campbell I, Qiu W, Haviv I. Genetic changes in tumour microenvironments. J Pathol 2011;223:450-8.

Cheng JB, Sedgewick AJ, Finnegan AI, Harirchian P, Lee J, Kwon S, et al. Transcriptional Programming of Normal and Inflamed Human Epidermis at Single-Cell Resolution. Cell reports 2018;25:871-83.

Cui Q, Wang B, Li K, Sun H, Hai T, Zhang Y, et al. Upregulating MMP-1 in carcinoma-associated fibroblasts reduces the efficacy of Taxotere on breast cancer synergized by Collagen IV. Oncology letters 2018;16:3537-44.

Desmouliere A, Geinoz A, Gabbiani F, Gabbiani G. Transforming growth factor-beta 1 induces alpha-smooth muscle actin expression in granulation tissue myofibroblasts and in quiescent and growing cultured fibroblasts. The Journal of cell biology 1993;122:103-11.

Ebert LM, Meuter S, Moser B. Homing and function of human skin gammadelta T cells and NK cells: relevance for tumor surveillance. J Immunol 2006;176:4331-6.

Fassy J, Tsalkitzi K, Goncalves-Maia M, Braud VM. A Real-Time Cytotoxicity Assay as an Alternative to the Standard Chromium-51 Release Assay for Measurement of Human NK and T Cell Cytotoxic Activity. Curr Protoc Immunol 2017a;118:7 42 1-7 12.

Fassy J, Tsalkitzi K, Salavagione E, Hamouda-Tekaya N, Braud VM. A real-time digital bio-imaging system to quantify cellular cytotoxicity as an alternative to the standard chromium-51 release assay. Immunology 2017b;150:489-94.

Fidler IJ. The pathogenesis of cancer metastasis: the 'seed and soil' hypothesis revisited. Nature reviews Cancer 2003;3:453-8.

Fong YW, Inouye C, Yamaguchi T, Cattoglio C, Grubisic I, Tjian R. A DNA repair complex functions as an Oct4/Sox2 coactivator in embryonic stem cells. Cell 2011;147:120-31.

Frechet M, Warrick E, Vioux C, Chevallier O, Spatz A, Benhamou S, et al. Overexpression of matrix metalloproteinase 1 in dermal fibroblasts from DNA repair-deficient/cancer-prone xeroderma pigmentosum group C patients. Oncogene 2008;27:5223-32.

Giglia G, Dumaz N, Drougard C, Avril MF, Daya-Grosjean L, Sarasin A. p53 mutations in skin and internal tumors of xeroderma pigmentosum patients belonging to the complementation group C. Cancer research 1998;58:4402-9.

Ho JJ, Cattoglio C, McSwiggen DT, Tjian R, Fong YW. Regulation of DNA demethylation by the XPC DNA repair complex in somatic and pluripotent stem cells. Genes Dev 2017;31:830-44.

Imai K, Matsuyama S, Miyake S, Suga K, Nakachi K. Natural cytotoxic activity of peripheral-blood lymphocytes and cancer incidence: an 11-year follow-up study of a general population. Lancet (London, England) 2000;356:1795-9.

Ishigami S, Natsugoe S, Tokuda K, Nakajo A, Che X, Iwashige H, et al. Prognostic value of intratumoral natural killer cells in gastric carcinoma. Cancer 2000;88:577-83.

Jiang L, Gonda TA, Gamble MV, Salas M, Seshan V, Tu S, et al. Global hypomethylation of genomic DNA in cancer-associated myofibroblasts. Cancer research 2008;68:9900-8.

Kalluri R, Zeisberg M. Fibroblasts in cancer. Nature reviews Cancer 2006;6:392-401.

Keijzer W, Jaspers NG, Abrahams PJ, Taylor AM, Arlett CF, Zelle B, et al. A seventh complementation group in excision-deficient xeroderma pigmentosum. Mutat Res 1979;62:183-90.

Kleijer WJ, Laugel V, Berneburg M, Nardo T, Fawcett H, Gratchev A, et al. Incidence of DNA repair deficiency disorders in western Europe: Xeroderma pigmentosum, Cockayne syndrome and trichothiodystrophy. DNA Repair (Amst) 2008;7:744-50.

Kraemer KH, Lee MM, Scotto J. Xeroderma pigmentosum. Cutaneous, ocular, and neurologic abnormalities in 830 published cases. Archives of dermatology 1987;123:241-50.

Le May N, Mota-Fernandes D, Velez-Cruz R, Iltis I, Biard D, Egly JM. NER factors are recruited to active promoters and facilitate chromatin modification for transcription in the absence of exogenous genotoxic attack. Molecular cell 2010;38:54-66.

Lehmann AR, McGibbon D, Stefanini M. Xeroderma pigmentosum. Orphanet J Rare Dis 2011;6:70.

Li A, Simmons PJ, Kaur P. Identification and isolation of candidate human keratinocyte stem cells based on cell surface phenotype. Proceedings of the National Academy of Sciences of the United States of America 1998;95:3902-7.

Li T, Yang Y, Hua X, Wang G, Liu W, Jia C, et al. Hepatocellular carcinoma-associated fibroblasts trigger NK cell dysfunction via PGE2 and IDO. Cancer Letters 2012;318:154-61.

Li Y, Wang Q, Chen S, Brown PH, Mariuzza RA. Structure of NKp65 bound to its keratinocyte ligand reveals basis for genetically linked recognition in natural killer gene complex. Proceedings of the National Academy of Sciences of the United States of America 2013;110:11505-10.

Mariani E, Facchini A, Honorati MC, Lalli E, Berardesca E, Ghetti P, et al. Immune defects in families and patients with xeroderma pigmentosum and trichothiodystrophy. Clinical and experimental immunology 1992;88:376-82.

Norris PG, Limb GA, Hamblin AS, Hawk JL. Impairment of natural-killer-cell activity in xeroderma pigmentosum. The New England journal of medicine 1988;319:1668-9.

Norris PG, Limb GA, Hamblin AS, Lehmann AR, Arlett CF, Cole J, et al. Immune function, mutant frequency, and cancer risk in the DNA repair defective genodermatoses xeroderma pigmentosum, Cockayne's syndrome, and trichothiodystrophy. The Journal of investigative dermatology 1990;94:94-100.

Otto AI, Riou L, Marionnet C, Mori T, Sarasin A, Magnaldo T. Differential behaviors toward ultraviolet A and B radiation of fibroblasts and keratinocytes from normal and DNA-repair-deficient patients. Cancer research 1999;59:1212-8.

Philippeos C, Telerman SB, Oules B, Pisco AO, Shaw TJ, Elgueta R, et al. Spatial and Single-Cell Transcriptional Profiling Identifies Functionally Distinct Human Dermal Fibroblast Subpopulations. The Journal of investigative dermatology 2018;138:811-25.

Qiu W, Hu M, Sridhar A, Opeskin K, Fox S, Shipitsin M, et al. No evidence of clonal somatic genetic alterations in cancer-associated fibroblasts from human breast and ovarian carcinomas. Nat Genet 2008;40:650-5.

Spreu J, Kienle EC, Schrage B, Steinle A. CLEC2A: a novel, alternatively spliced and skin-associated member of the NKC-encoded AICL-CD69-LLT1 family. Immunogenetics 2007;59:903-12.

Spreu J, Kuttruff S, Stejfova V, Dennehy KM, Schittek B, Steinle A. Interaction of C-type lectin-like receptors NKp65 and KACL facilitates dedicated immune recognition of human keratinocytes. Proceedings of the National Academy of Sciences of the United States of America 2010;107:5100-5.

Stary A, Sarasin A. The genetics of the hereditary xeroderma pigmentosum syndrome. Biochimie 2002;84:49-60.

Valin A, Barnay-Verdier S, Robert T, Ripoche H, Brellier F, Chevallier-Lagente O, et al. PTCH1 +/- dermal fibroblasts isolated from healthy skin of Gorlin syndrome patients exhibit features of carcinoma associated fibroblasts. PloS one 2009;4:e4818.

Zelenay S, van der Veen AG, Bottcher JP, Snelgrove KJ, Rogers N, Acton SE, et al. Cyclooxygenase-Dependent Tumor Growth through Evasion of Immunity. Cell 2015;162:1257-70.

Ziani L, Safta-Saadoun TB, Gourbeix J, Cavalcanti A, Robert C, Favre G, et al. Melanoma-associated fibroblasts decrease tumor cell susceptibility to NK cell-mediated killing through matrix-metalloproteinases secretion. Oncotarget 2017;8:19780-94.

FIGURE LEGENDS

Figure 1. Transcriptomic analysis of WT and XP-C fibroblasts cultured in 3D collagen matrices. (**a**) Principal component analysis (PCA) showing the clustering of WT and XP-C fibroblasts. (**b**) Volcano plot highlighting the 22 differentially expressed genes (DEG) between WT and XP-C fibroblasts. On the upper left quadrant, upregulated mRNAs in WT fibroblasts and on the upper right quadrant, downregulated mRNAs in WT fibroblasts are shown. (**c**) Boxplot of log2 intensity *CLEC2A* variant 1and 2 mRNA levels in WT (n=3) and XP-C (n=3) fibroblasts.

Figure 2. CLEC2A expression in primary fibroblasts isolated from healthy and XP-C individuals. (**a**) Relative *CLEC2A* mRNA transcript levels in WT and XP-C fibroblasts (F-WT, F-XP-C), determined by quantitative RT-PCR. Data represent mean ± SEM of five or eight cell lines per group. ***p <0,001 Mann-Whitney *U*-test. (**b**) Representative histograms of CLEC2A expression in WT and XP-C fibroblasts determined by flow cytometry. (**c**) Frequency of CLEC2A positive cells in WT and XP-C fibroblasts as determined by flow cytometry. Data are representative of three independent experiments with five or eight cell lines per group. ***p <0,001 Mann-Whitney *U*-test.

Figure 3. CLEC2A expression in dermal CAFs from SCC. (**a**) α-SMA and DAPI immunofluorescence staining of WT and XP-C fibroblasts and primary isolated dermal CAFs from SCC. Data are representative of three independent experiments. Scale bar = 100µm. (**b**) Relative *CLEC2A* mRNA transcript levels in WT fibroblasts and dermal CAFs determined by quantitative RT-PCR. Data represent mean ± SEM of three independent experiments. ***$p\leq$0,001 Mann-Whitney *U*-test. (**c**) Representative histograms of *CLEC2A* expression in WT fibroblasts and dermal CAFs determined by flow cytometry. Three independent experiments were performed.

Figure 4. Regulation of CLEC2A expression by SCC12_conditioned medium (SCC12_CM) in WT fibroblasts. (**a**) α-SMA immunofluorescence staining of WT fibroblasts after stimulation with SCC12_CM for five days. Scale bar = 100µm. (**b**) Relative *CLEC2A* mRNA transcripts levels in WT fibroblasts stimulated by SCC12_CM. Data represent mean ± SEM of five different CM. ***p*≤0,01 Mann-Whitney *U*-test. (**c**) Representative histograms of CLEC2A expression on WT fibroblasts stimulated or not by SCC12_CM as determined by flow cytometry. Three independent experiments were performed. (**d**) Representative histograms of CLEC2A expression on WT fibroblasts stimulated with 10 ng/ml human recombinant IL-1α, IL-1β and TNF-α for 48 h. Three independent experiments were performed. (e) Representative histograms of CLEC2A expression on WT fibroblasts stimulated by SCC12_CM depleted or not of IL-1α, IL-1β and TNF-α. Control using Prot-G-sepharose bead was included. Two independent experiments were performed.

Figure 5. *KLRF2* and *CLEC2A* transcript expression in healthy skin.

(**a**) Relative *KRLF2* mRNA transcript levels in the indicated cells. Data represent mean ± SD of triplicates ***p*≤0,01 Mann-Whitney *U*-test. (**b**) In situ hybridization using RNAscope® technology on FFPE sections of human healthy or XP-C skin and counterstaining with Haematoxylin:. upper panel, (RNAscope® Negative Control Probe – DapB); middle and lower panels, (RNAscope® CLEC2A Probe – blue and KLRF2 Probe-red). Scale bar = 20 µm.

Figure 6. Assessment of the impact of CLEC2A on the ability of NK cells to control invasion in a 3D-NK immunocompetent culture model. (**a**) Schematic representation of the model. (**b**) Time-course NK cell-mediated lysis of SCC12 and K562 cells (left) and WT or XP-C fibroblasts and K562 target cells in presence of indomethacin (100µM) (right), at an effector-to-target ratio 5:1. (**c**) Representative-hematoxylin and eosin (H&E) staining of SCC12 cell invasion in WT, XP-C and CAF 3D-NK immunocompetent organotypic skin cultures in

absence or presence of NK cells, with anti-CLEC2A blocking antibody (OMA1) or isotype Ig. Scale bar = 200µm. (**d**) Quantification of SCC12 invasion rate in the aforementioned conditions shown as box plots. ***$p \leq 0{,}001$ Tukey's test in one-way ANOVA. Two independent experiments were performed.

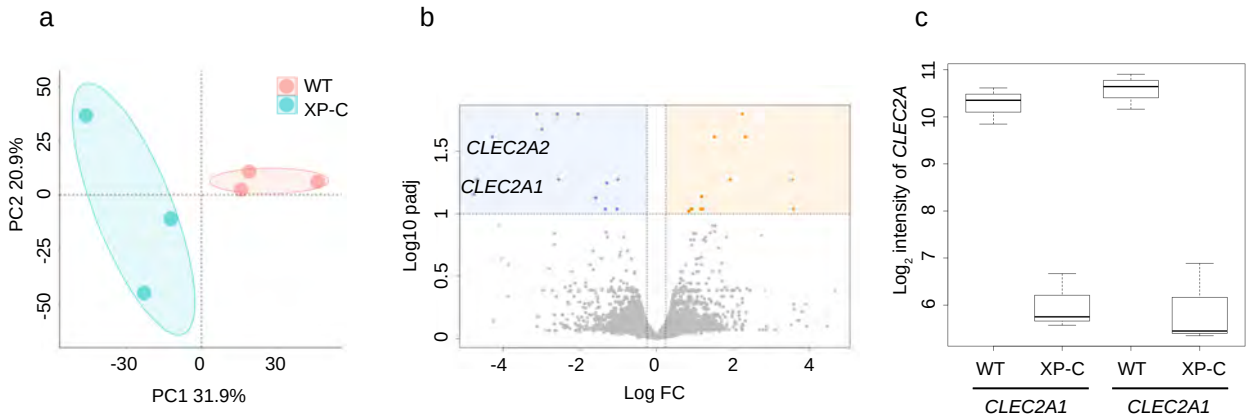
a
b
c
WT
XP-C
PC2 20.9%
PC1 31.9%
-30
0
30
50
25
0
-25
-50
CLEC2A2
CLEC2A1
Log10 padj
Log FC
-4
-2
0
2
4
0
0.5
1
1.5
Log2 intensity of CLEC2A
6
7
8
9
10
11
WT
XP-C
WT
XP-C
CLEC2A1
CLEC2A1

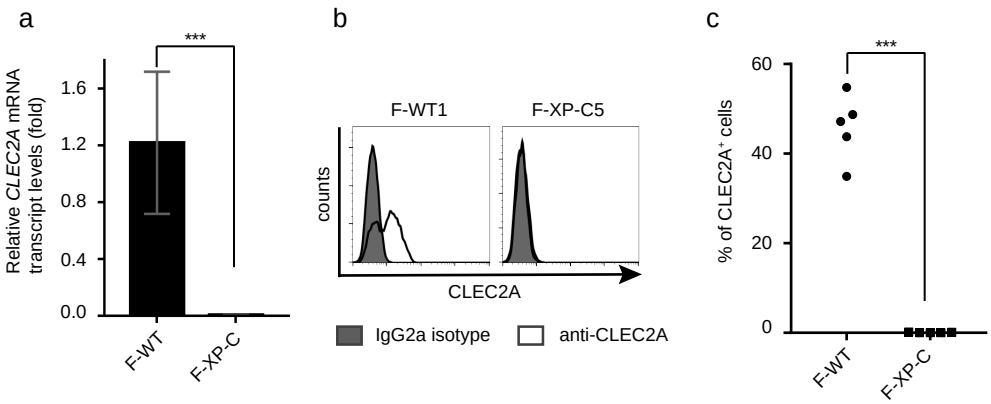
a
***
Relative CLEC2A mRNA transcript levels (fold)
1.6
1.2
0.8
0.4
0.0
F-WT
F-XP-C
b
F-WT1
F-XP-C5
counts
CLEC2A
IgG2a isotype
anti-CLEC2A
c
***
% of CLEC2A+ cells
60
40
20
0
F-WT
F-XP-C

a

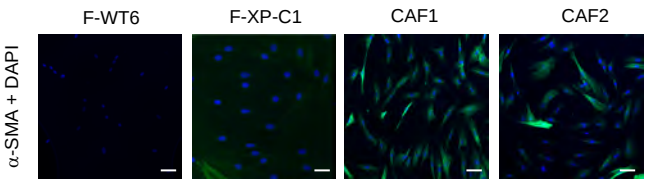
F-WT6
F-XP-C1
CAF1
CAF2
α-SMA + DAPI

b

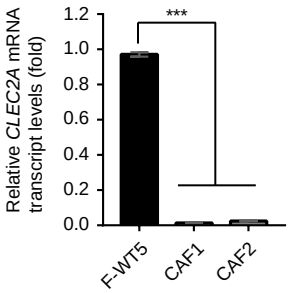
***
1.2
1.0
0.8
0.6
0.4
0.2
0.0
Relative CLEC2A mRNA transcript levels (fold)
F-WT5
CAF1
CAF2

c

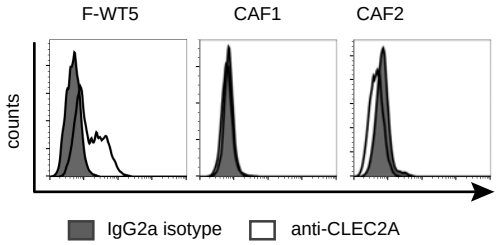
F-WT5
CAF1
CAF2
counts
IgG2a isotype
anti-CLEC2A

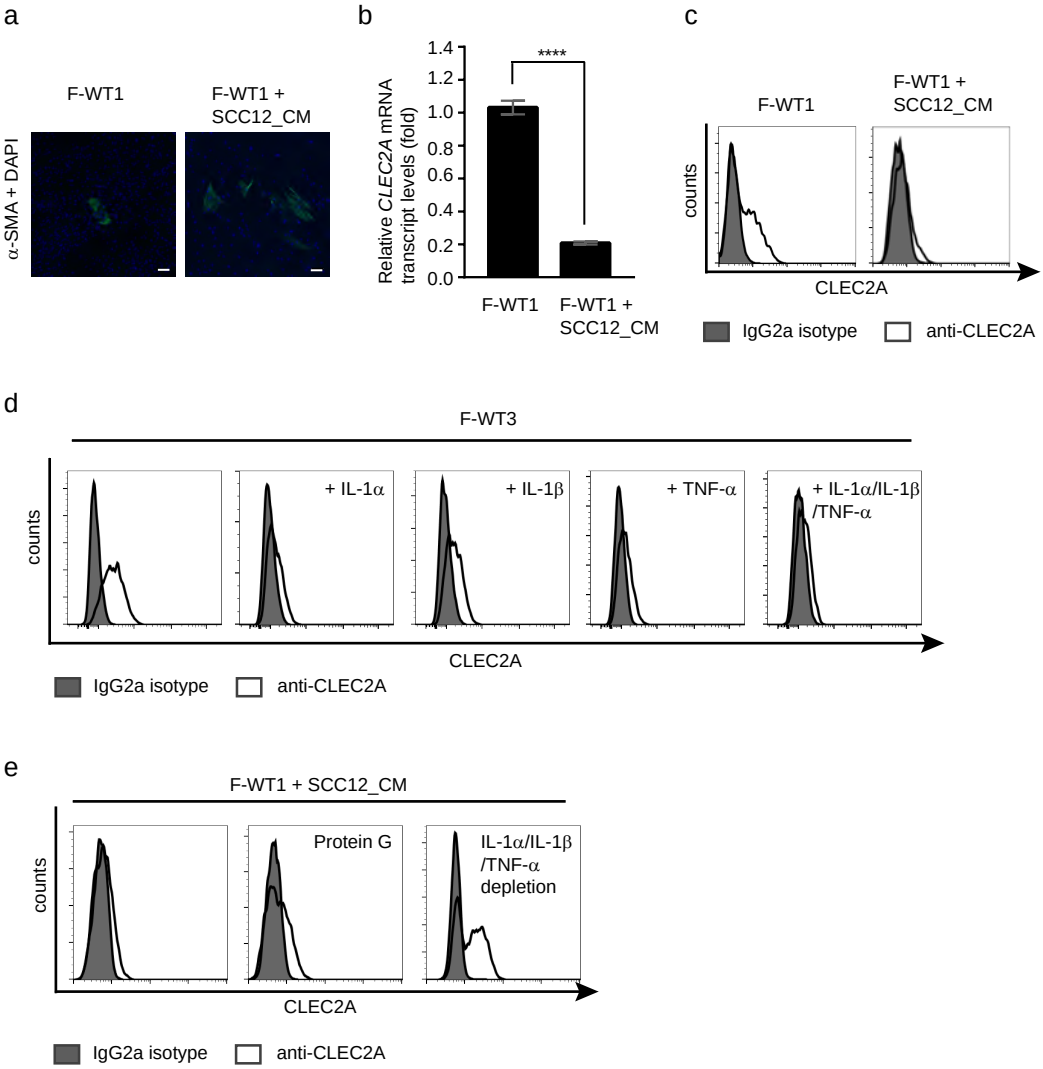
a
F-WT1
F-WT1 +
SCC12_CM
α-SMA + DAPI
b
Relative CLEC2A mRNA
transcript levels (fold)
1.4
1.2
1.0
0.8
0.6
0.4
0.2
0.0
****
F-WT1
F-WT1 +
SCC12_CM
c
F-WT1
F-WT1 +
SCC12_CM
counts
CLEC2A
IgG2a isotype
anti-CLEC2A
d
F-WT3
counts
+ IL-1α
+ IL-1β
+ TNF-α
+ IL-1α/IL-1β
/TNF-α
CLEC2A
IgG2a isotype
anti-CLEC2A
e
F-WT1 + SCC12_CM
counts
Protein G
IL-1α/IL-1β
/TNF-α
depletion
CLEC2A
IgG2a isotype
anti-CLEC2A

a

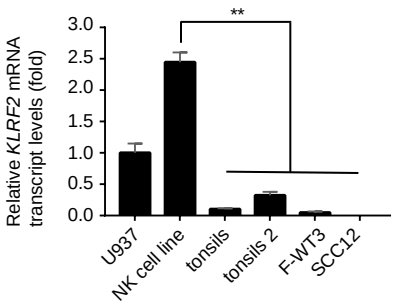
**
3.0
2.5
2.0
1.5
1.0
0.5
0.0
Relative KLRF2 mRNA transcript levels (fold)
U937
NK cell line
tonsils
tonsils 2
F-WT3
SCC12

b

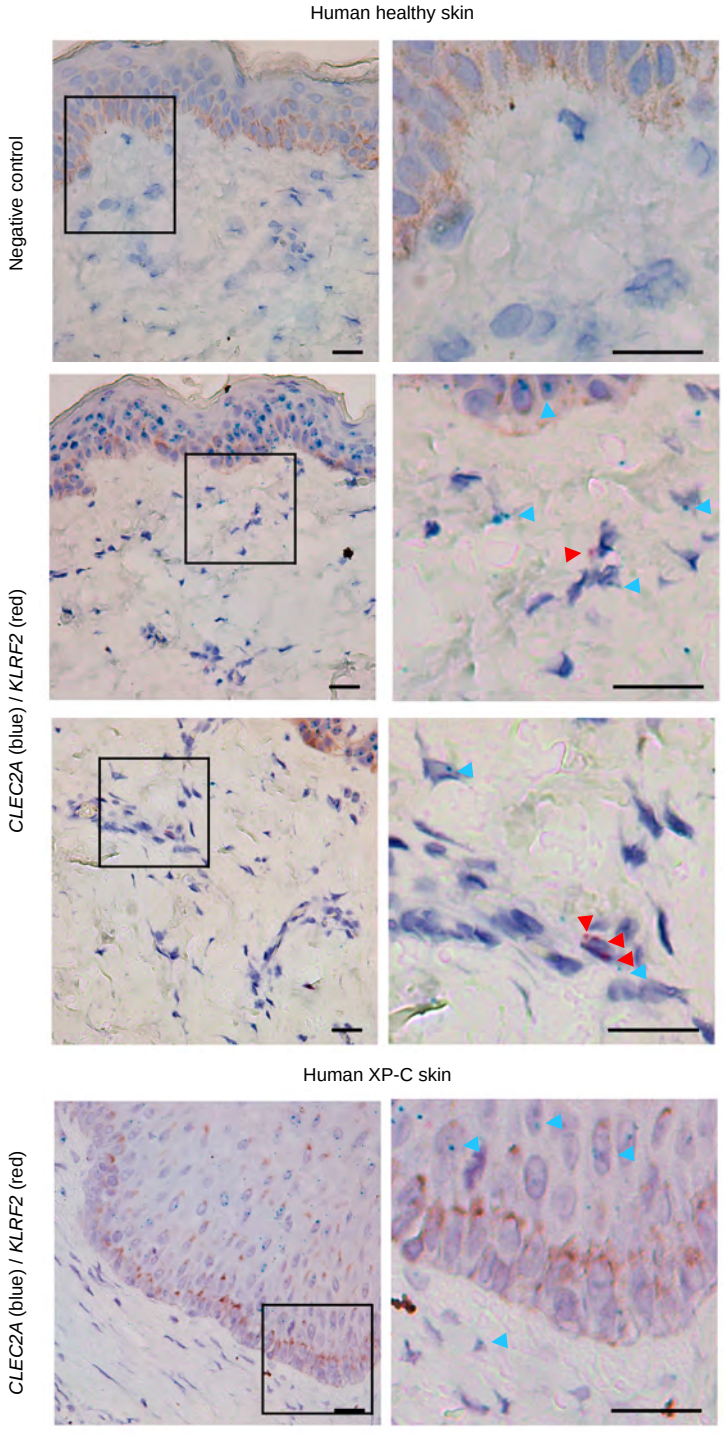
Human healthy skin
Negative control
CLEC2A (blue) / KLRF2 (red)
Human XP-C skin
CLEC2A (blue) / KLRF2 (red)

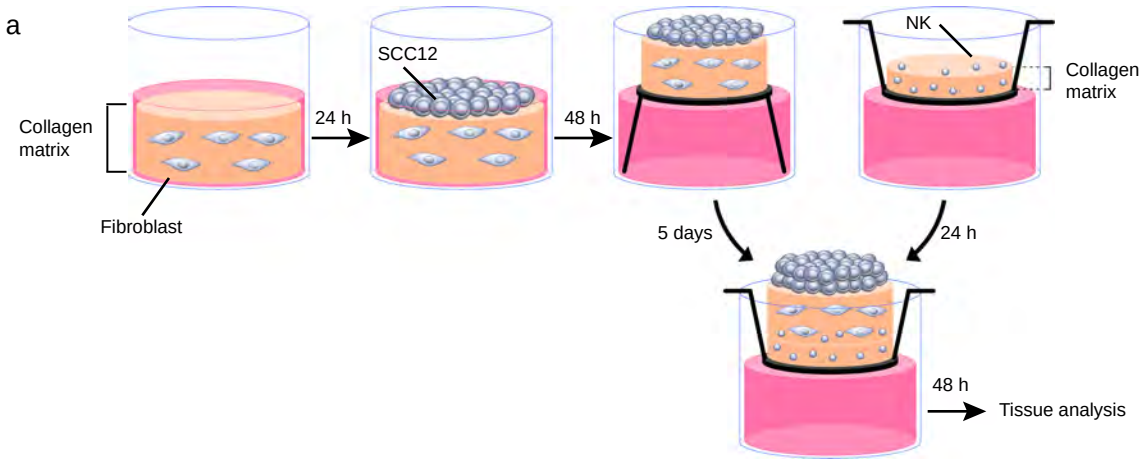
a
Collagen matrix
Fibroblast
24 h
SCC12
48 h
NK
Collagen matrix
5 days
24 h
48 h
Tissue analysis

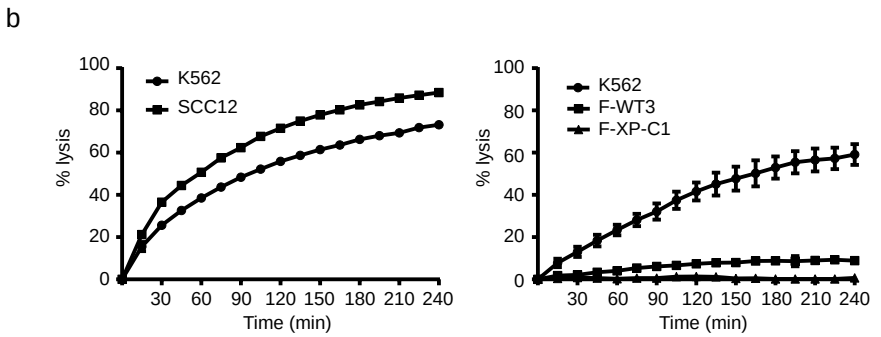
b
% lysis
K562
SCC12
Time (min)
K562
F-WT3
F-XP-C1
Time (min)

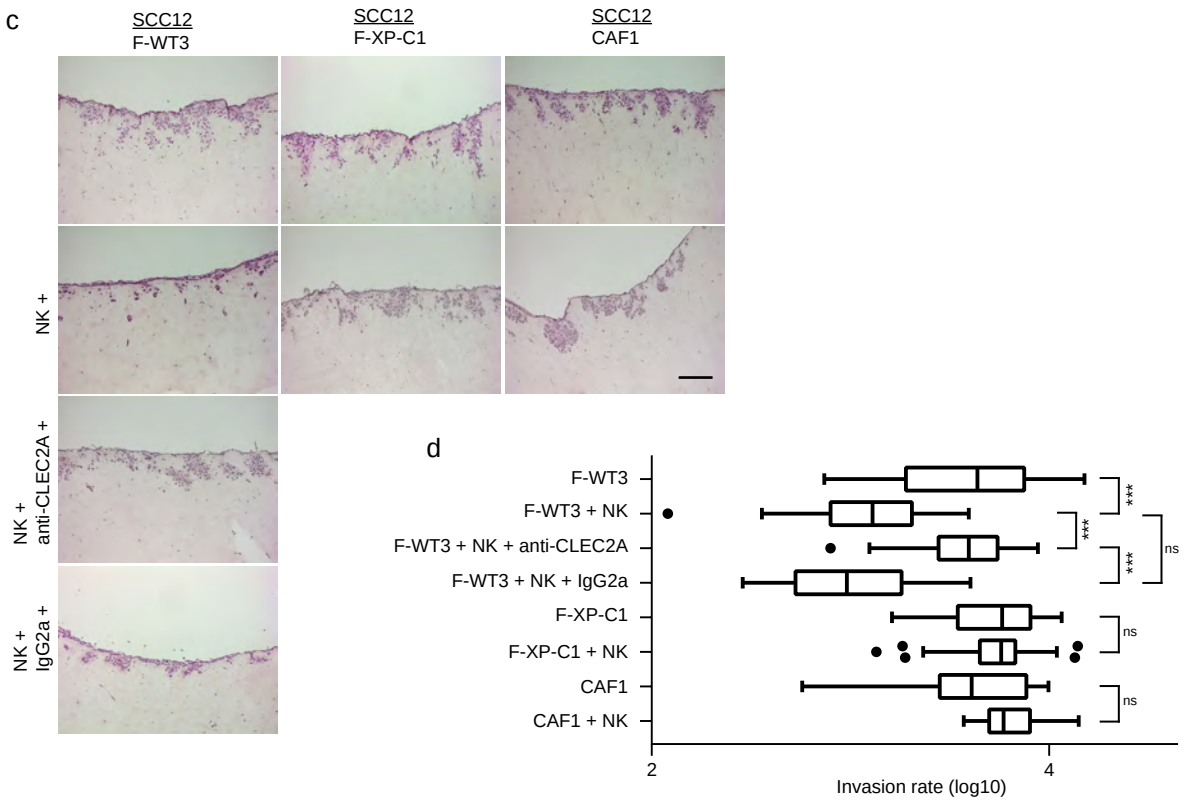
c
SCC12
F-WT3
SCC12
F-XP-C1
SCC12
CAF1
NK +
NK + anti-CLEC2A +
NK + IgG2a +
d
F-WT3
F-WT3 + NK
F-WT3 + NK + anti-CLEC2A
F-WT3 + NK + IgG2a
F-XP-C1
F-XP-C1 + NK
CAF1
CAF1 + NK
***
***
***
ns
ns
ns
Invasion rate (log10)

Supplementary Material

NK cell and fibroblast-mediated regulation of skin squamous cell carcinoma invasion by CLEC2A is compromised in Xeroderma Pigmentosum

Maria Gonçalves-Maia[1], Yannick Gache[1,7], Miguel Basante[1,2,7], Estelle Cosson[3], Emie Salavagione[3], Margot Muller[1], Françoise Bernerd[4], Marie Françoise Avril[5], Sébastien Schaub[2], Alain Sarasin[6], Véronique M. Braud[3,8], Thierry Magnaldo[1,8]

Supplementary Figure 1. Skin primary fibroblast phenotype. **(a)** Representative CD90 staining in skin primary fibroblasts. **(b)** *CLEC2A* transcript variants were amplified by RT-PCR in F-WT6 fibroblast (lane 1), U937 cell line (lane 2), F-XP-C3 fibroblast (lane 3), RT negative control (lane 4), PCR buffer negative control (lane 5). **(c)** CLEC2A expression in F-WT3 fibroblasts, determined by imaging flow cytometry. Data is representative of two independent experiments.

a

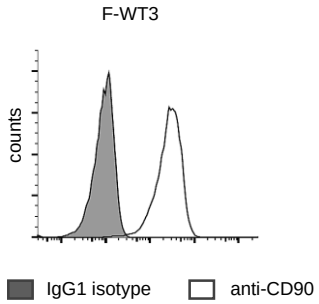
F-WT3
counts
IgG1 isotype
anti-CD90

b

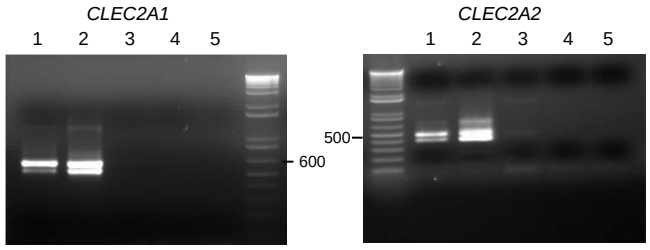
CLEC2A1
1 2 3 4 5
CLEC2A2
1 2 3 4 5
500
600

c

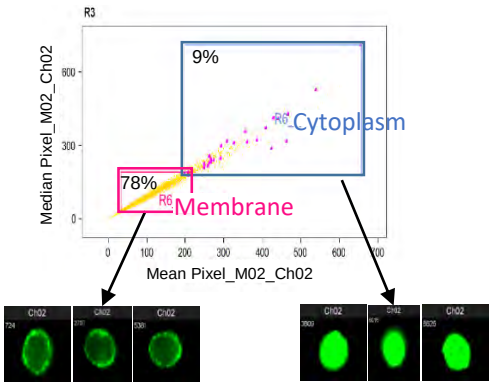
R3
9%
Cytoplasm
78%
Membrane
Median Pixel_M02_Ch02
Mean Pixel_M02_Ch02

Supplementary Figure 2. Expression of CLEC2A in XP-C-reverted fibroblasts. (**a**) Expression of XPC protein in WT, XP-C and transduced XP-C fibroblasts determined by Western blot: F-WT1 fibroblast (lane 1), F-WT3 fibroblast (lane 2), F-XP-C3 fibroblast (lane 3), F-XP-C3+XPC reverted fibroblast (lane 4), F-XP-C5 fibroblast (lane 5), F-XP-C5+XPC reverted fibroblast (lane 6). Anti-GAPDH antibody was used as a loading control. (**b**) Measurement of UDS by EdU incorporation 2 h after 500 J/cm^2 UVB in WT, XP-C and transduced XP-C fibroblasts shows that genetically corrected XP-C fibroblasts recovered full NER capacity. Bar = 100 μm. (**c**) Relative *CLEC2A* mRNA transcripts levels in WT, XP-C, and XP-C-reverted fibroblasts determined by quantitative RT-PCR. Data represent mean ± SEM of two independent experiments. ***p <0,001 Mann-Whitney *U*-test.

a

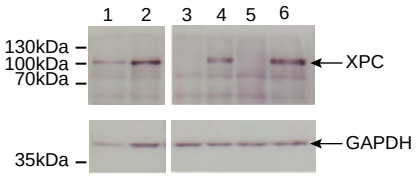
1 2 3 4 5 6
130kDa
100kDa
70kDa
XPC
35kDa
GAPDH

b

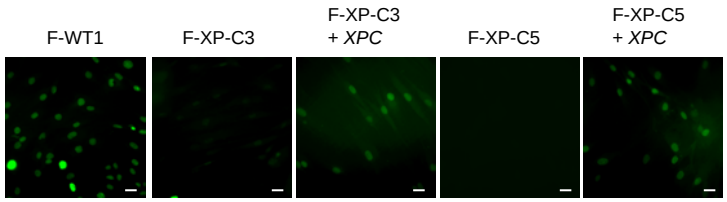
F-WT1
F-XP-C3
F-XP-C3
+ XPC
F-XP-C5
F-XP-C5
+ XPC

C

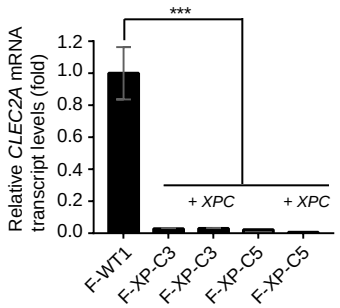
***
Relative CLEC2A mRNA transcript levels (fold)
1.2
1.0
0.8
0.6
0.4
0.2
0.0
+ XPC
+ XPC
F-WT1
F-XP-C3
F-XP-C3
F-XP-C5
F-XP-C5

Supplementary Figure 3. CLEC2A expression in dermal CAFs from BCC. (**a**) Relative *CLEC2A* mRNA transcript levels in WT fibroblasts and dermal CAFs from BCC determined by quantitative RT-PCR. Data represent mean ± SD of triplicates of one WT fibroblasts and three CAF_BCC cell lines. ***p<0,001 Mann-Whitney U-test. (**b**) Representative histograms of CLEC2A expression in WT fibroblasts and dermal CAFs from BCC, determined by flow cytometry. Three independent experiments were performed.

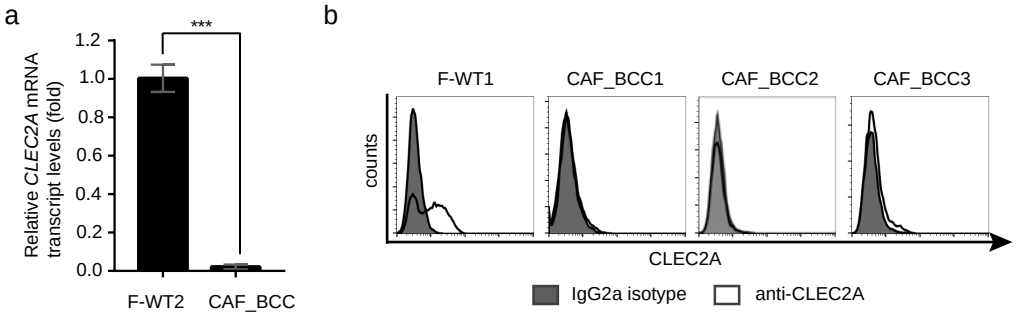
a
***
1.2
1.0
0.8
0.6
0.4
0.2
0.0
Relative CLEC2A mRNA transcript levels (fold)
F-WT2
CAF_BCC
b
F-WT1
CAF_BCC1
CAF_BCC2
CAF_BCC3
counts
CLEC2A
IgG2a isotype
anti-CLEC2A

Supplementary Figure 4. CLEC2A expression in WT fibroblasts after conditioned medium and TGF-β1 stimulation. Relative *CLEC2A* mRNA transcripts levels in WT fibroblasts stimulated or not for five days with (**a**) WT fibroblast or (**b**) WT keratinocyte culture medium. (**c**) Relative *CLEC2A* mRNA transcript levels in WT fibroblasts after stimulation for 48 h with 2ng/mL TGF-β1 or SCC12_CM, with or without 10μg/mL anti-TGF-β neutralizing antibody, determined by quantitative RT-PCR. (**d**) α-SMA immunofluorescence staining of WT fibroblasts after stimulation for 48 h with TGF-β1. Data are representative of two independent experiments. Bar = 100 μm.

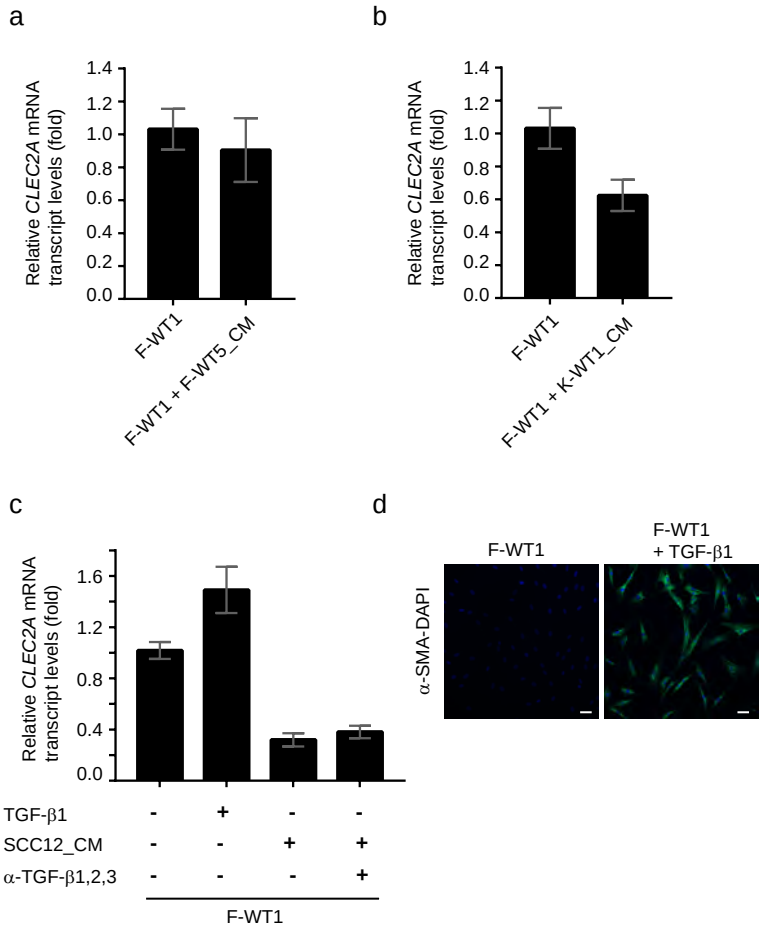
a
Relative CLEC2A mRNA transcript levels (fold)
1.4
1.2
1.0
0.8
0.6
0.4
0.2
0.0
F-WT1
F-WT1 + F-WT5_CM
b
Relative CLEC2A mRNA transcript levels (fold)
F-WT1
F-WT1 + K-WT1_CM
c
Relative CLEC2A mRNA transcript levels (fold)
1.6
1.2
0.8
0.4
0.0
TGF-β1 - + - -
SCC12_CM - - + +
α-TGF-β1,2,3 - - - +
F-WT1
d
F-WT1
F-WT1 + TGF-β1
α-SMA-DAPI

Supplementary Figure 5. *KLRF2* and *CLEC2A* expression profiles. (**a**) *KLRF2* and (**b**) *CLEC2A* expression profiles in human tissues (upper panel) and in human cell lines (lower panel). RNA-seq data generated by Human Protein Atlas (HPA) database is reported in 'Transcript Per Million' (TPM) as the sum of the TPM values of all its protein-coding transcripts. RNA-seq data generated by the Genotype-Tissue Expression (GTEx) project is reported as average RPKM (reads per kilobase per million mapped reads). Normal distribution across the dataset is visualized with box plots, shown as median and 25th and 75th percentiles. Points are displayed as outliers if they are above or below 1.5 times the interquartile range. RPKM values of the individual samples are presented next to the box plot. These data are extracted from https://www.proteinatlas.org/.

a

KLRF2

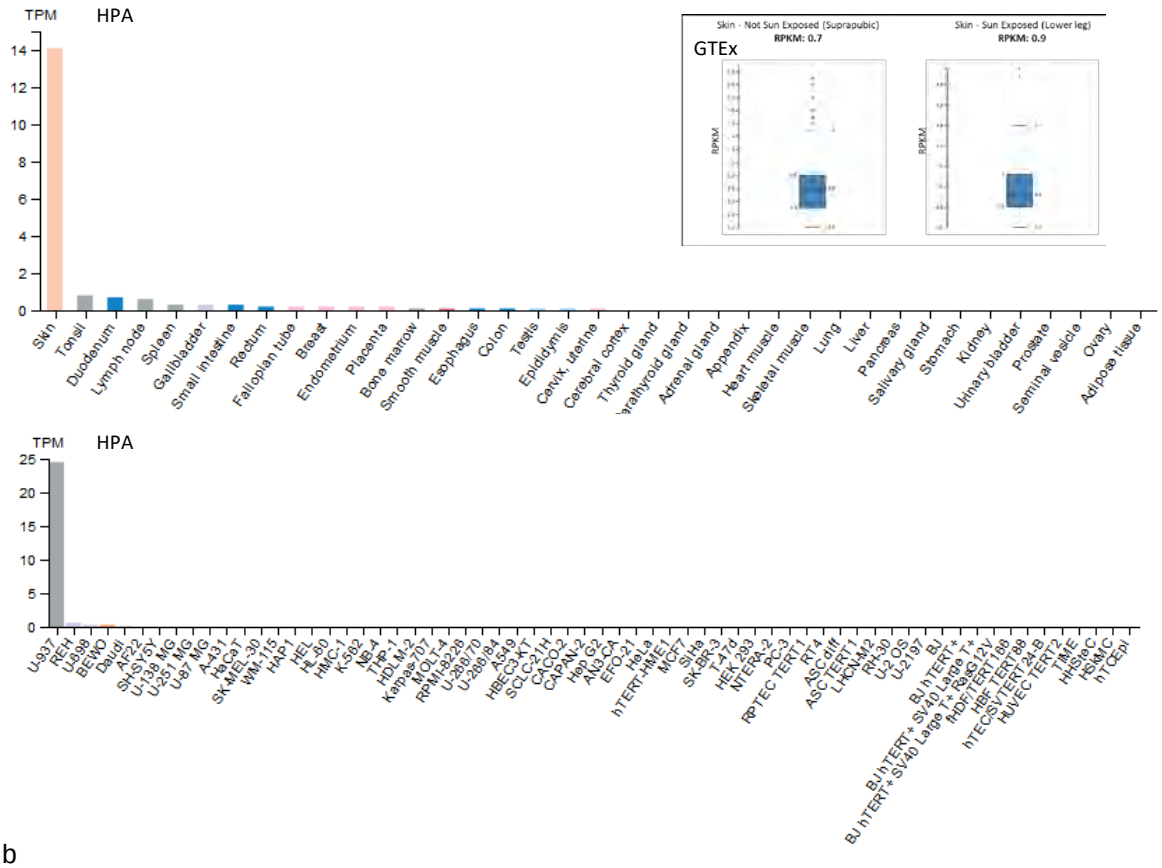

b

CLEC2A

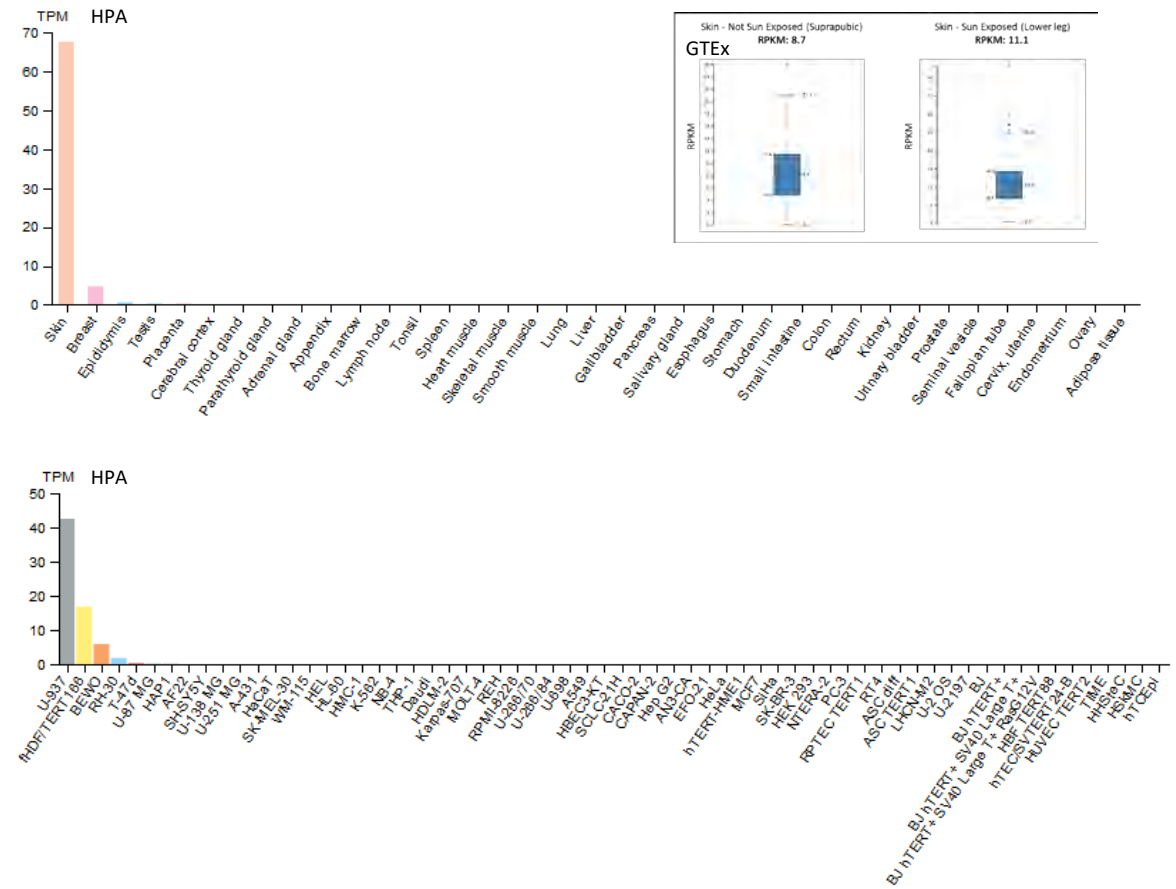

Supplementary Figure 6. Phenotype of cells used in the 3D immunocompetent culture model. (**a**) NK cell line phenotype determined by flow cytometry using anti-CD56, anti-CD16, anti-NKG2D, and anti-NKp46 antibodies compared to fluorescence minus one control (FMO) stainings. (**b**) MHC I cell surface expression in WT, XP-C fibroblasts and SCC12 cells determined by flow cytometry using anti-MHC I antibody, clone W6/32 compared to isotype Ig control. (**c**) Representative flow cytometry histograms of CLEC2A expression in cells used in the 3D dermal culture. Data are representative of three independent experiments.

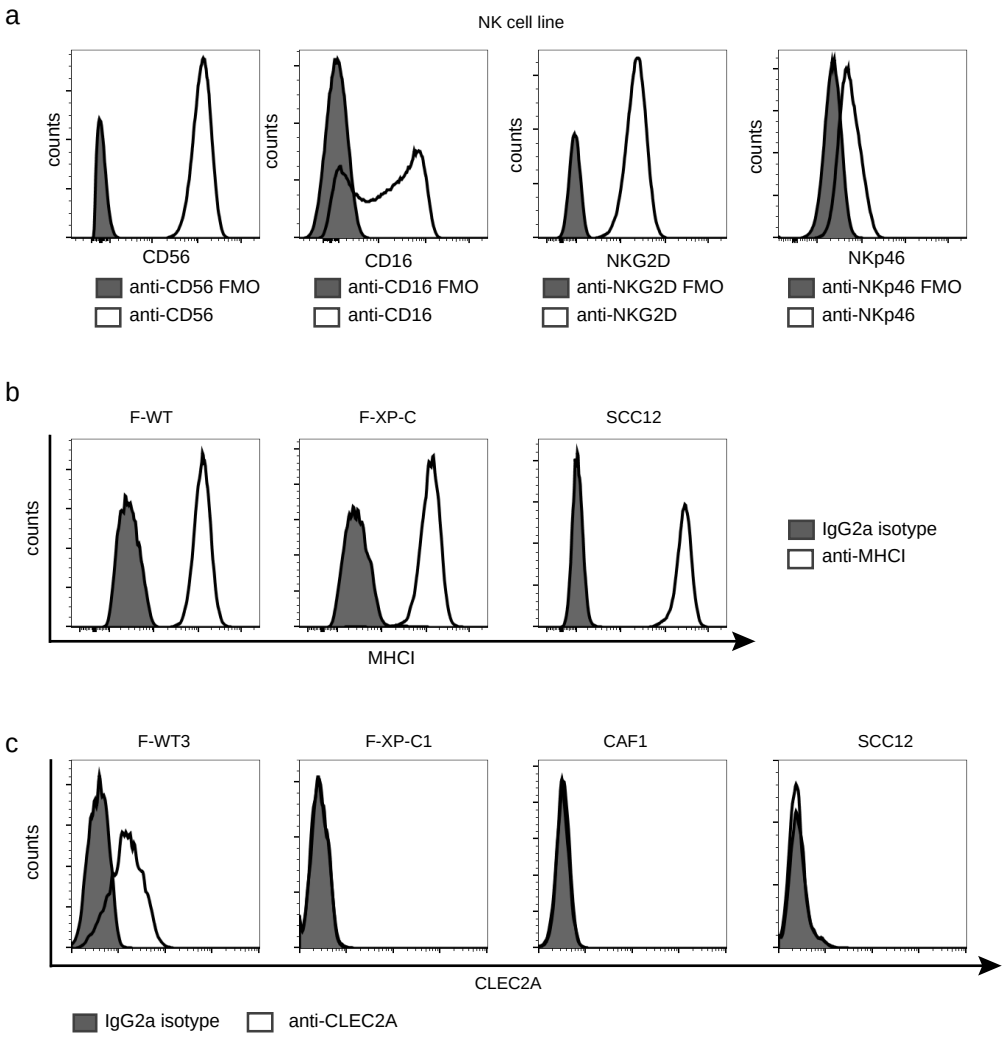
a
NK cell line
counts
CD56
anti-CD56 FMO
anti-CD56
CD16
anti-CD16 FMO
anti-CD16
NKG2D
anti-NKG2D FMO
anti-NKG2D
NKp46
anti-NKp46 FMO
anti-NKp46
b
F-WT
F-XP-C
SCC12
MHCI
IgG2a isotype
anti-MHCI
c
F-WT3
F-XP-C1
CAF1
SCC12
CLEC2A
IgG2a isotype
anti-CLEC2A

Supplementary Figure 7. Assessment of the impact of CLEC2A on the ability of NK cells to control invasion in a 3D-NK immunocompetent culture model. Representative hematoxylin and eosin (H&E) staining of SCC12 cell invasion in WT, XP-C and CAF 3D-NK immunocompetent organotypic skin cultures in absence or presence of NK cells, with anti-CLEC2A blocking antibody (OMA1) or isotype Ig. Bar = 200µm. Zoom are shown.

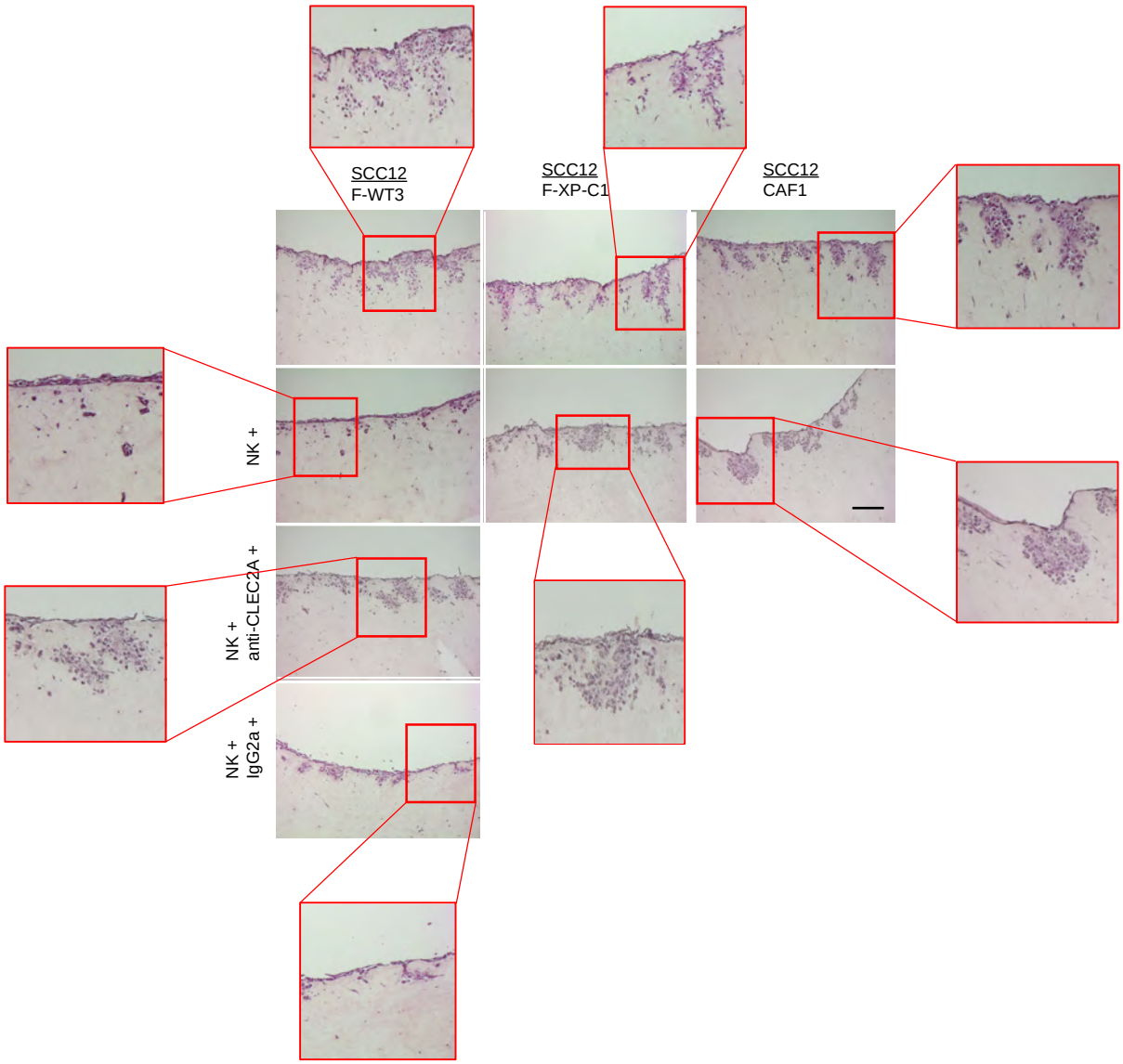
SCC12
F-WT3
SCC12
F-XP-C1
SCC12
CAF1
NK +
NK +
anti-CLEC2A +
NK +
IgG2a +

Supplementary Table S1. 22 differentially expressed genes between WT and XP-C fibroblasts

GeneName	xpc_as433	xpc_as798	xpc_as148	wt_ftm5	wt_ftm1	wt_fh122	baseMean xpc	baseMean wt	logFC xpc_wt	Adj.P.val xpc_wt	B xpc_wt
BST2	5,5025	5,4540	6,2463	9,4801	11,3199	10,6729	5,7343	10,4910	-4,7567	0,0700	1,9563
CLEC2A	6,8857	5,3487	5,4485	10,9056	10,6447	10,1662	5,8943	10,5722	-4,6779	0,0532	2,1817
CLEC2A	6,6677	5,7504	5,5724	10,6162	10,3538	9,8480	5,9968	10,2727	-4,2759	0,0241	2,6423
RSPO3	7,8106	7,9342	7,9687	11,2786	10,6459	11,1118	7,9045	11,0121	-3,1076	0,0159	3,2261
RSPO3	8,2050	8,2527	8,3432	11,5624	10,7674	11,4308	8,2669	11,2535	-2,9866	0,0210	2,8119
TBX5	5,8601	5,4998	5,9386	8,1331	8,4030	8,5422	5,7662	8,3595	-2,5933	0,0159	3,0254
GALNT14	7,9420	7,4939	7,8585	10,2728	9,9094	10,7702	7,7648	10,3175	-2,5527	0,0532	2,1438
TBX5-AS1	5,5025	5,1931	5,2792	7,3144	7,3212	7,4771	5,3249	7,3709	-2,0459	0,0159	3,1670
DUSP6	11,1729	11,0631	11,4087	12,6984	12,6268	13,0909	11,2149	12,8054	-1,5905	0,0743	1,8711
ENST00000369474	6,5157	6,6269	6,8031	8,2050	7,9391	7,7966	6,6486	7,9802	-1,3317	0,0914	1,7141
SCN1B	5,9619	6,2495	6,0715	7,2621	7,3750	7,5203	6,0943	7,3858	-1,2915	0,0566	2,0850
GREB1L	8,1007	7,9806	8,2084	9,1548	8,9981	9,2157	8,0966	9,1229	-1,0263	0,0915	1,6436
GREB1L	7,1900	7,2186	7,2980	8,1826	8,2817	8,2392	7,2355	8,2345	-0,9990	0,0532	2,1575
PITX1	9,5760	9,5470	9,1454	5,3129	6,1413	6,0205	9,4228	5,8249	3,5979	0,0185	2,9066
ZMAT4	10,3849	9,8579	9,5832	5,6865	7,1807	6,2463	9,9420	6,3712	3,5708	0,0915	1,6091
PRDM16	9,9621	8,8009	8,6707	5,5648	5,5949	5,5949	9,1446	5,5849	3,5597	0,0532	2,1508
ENST00000424493	7,8898	7,7313	8,0557	5,2095	5,7835	5,7027	7,8923	5,5652	2,3270	0,0241	2,6321
HOTAIR	7,9124	7,4939	7,6369	5,3487	5,6073	5,3866	7,6811	5,4475	2,2335	0,0159	3,0111
HOXC10	9,8085	10,0101	9,9999	7,7510	7,9039	8,3714	9,9395	8,0088	1,9307	0,0532	2,1992
LINC00982	6,8455	6,7627	6,9099	5,4066	5,1531	5,4066	6,8393	5,3221	1,5173	0,0241	2,7033
COL5A1	12,0081	12,1632	11,9661	10,6598	11,0594	10,7978	12,0458	10,8390	1,2068	0,0915	1,6084
LOC90246	7,8329	7,6730	7,7604	6,4094	6,5825	6,7358	7,7554	6,5759	1,1796	0,0726	1,9101
COL14A1	12,0220	11,9968	12,3654	10,9539	11,0195	10,9403	12,1281	10,9712	1,1569	0,0915	1,6084
LOC100130372	6,8857	6,8978	6,9327	6,0094	6,0715	5,8559	6,9054	5,9789	0,9265	0,0915	1,6803
PDLIM7	12,1877	12,0745	12,2514	11,2963	11,2015	11,2683	12,1712	11,2554	0,9158	0,0914	1,7270
PDLIM7	10,6817	10,6504	10,7961	9,8433	9,8265	9,9145	10,7094	9,8614	0,8480	0,0953	1,5539

For RSPO3, GREB1L, PDLIM7 two probe sets for the same gene sit side by side.
CLEC2A NM_001130711 corresponds to CLEC2A transcript variant 1; CLEC2A NM_207375 corresponds to CLEC2A transcript variant 2.
Cutoffs: log FC (≥0.8 and ≤-0.8); adj.p.value (<0.1); B (B> 0)

Supplementary Table S2. Patients and cell characteristics

Patients cells	Origin	Cell lines	Phenotype	XP-C mutation	Age at biopsy	Clinical characteristics	Onset of tumors
TM1	Caucasian	F-WT1/K-TM1	NA	NA	40 years	NA	NA
FH29	Caucasian	F-WT2	NA	NA	30 years	NA	NA
FH84	Black	F-WT3	NA	NA	28 years	NA	NA
FMD	Caucasian	F-WT4	NA	NA	16 years	NA	NA
TM5	Caucasian	F-WT5	NA	NA	25 years	NA	NA
FH122	Caucasian	F-WT6	NA	NA	19 years	NA	NA
SK	Caucasian	X	NA	NA	7 years	NA	NA
YF29	ND	X	NA	NA	newborn	NA	NA
AS148	Caucasian	F-XP-C1	XP-C	c.1643_1644delTG; p.Val548Alafsx25	12 years	Multiple BCCs and SCCs, face and exposed areas	9 years
AS188	Caucasian	F-XP-C2	XP-C	c.1643_1644delTG; p.Val548Alafsx25	7 years	Several SCC and 1 BCC on the face	ND
AS373	Caucasian	X	XP-C	c.1643_1644delTG; p.Val548Alafsx25	4 years	1 facial BCC	2 years
AS399	Caucasian	X	XP-C	ND	9 years	ND	5 years
AS433	Caucasian	F-XP-C3	XP-C	c.1643_1644delTG; p.Val548Alafsx25	2 months	ND	ND
AS629	Caucasian	X	XP-C	c.1643_1644delTG; p.Val548Alafsx25	8 years	ND	ND
AS703	ND	CAF_BCC1	NA	NA	77 years	BCC	ND
AS704	Caucasian	F-XP-C4	XP-C	c.1243C>T p.Arg415X	ND	ND	ND
AS728	Caucasian	X	NA	NA	37 years	NA	NA
AS749	ND	CAF_BCC2	NA	NA	84 years	BCC	ND
AS763	ND	CAF_BCC3	NA	NA	80 years	BCC	ND
AS798	Caucasian	F-XP-C5	XP-C	c.1643_1644delTG; p.Val548Alafsx25	2 years	Photoaging (hands), ephelides, Actinic keratosis	NA
AS844	Caucasian	F-XP-C6	XP-C	IVS12-1G > C	ND	ND	ND
AS860	Caucasian	F-XP-C7	XP-C	c.658C>T homoz p.Arg220X	ND	ND	ND
AS875	Caucasian	F-XP-C8	XP-C	ND	20 years	ND	ND
TM23	Caucasian	CAF1	NA	NA	82 years	SCC in left ankle	ND
TM24	Caucasian	CAF2	NA	NA	96 years	SCC	ND

NA, not applicable; ND, not determined; F, fibroblasts; K, keratinocytes

Supplementary Methods

RNA extraction. 3D-dermal cultures were frozen in liquid nitrogen, and then disrupted and solubilized in Qiazol reagent (Qiagen) using a gentleMACS^{TM} Dissociator (Miltenyi Biotech) with M tubes and the RNA_02 program recommended by the manufacturer (Miltenyi Biotech). Total RNAs were extracted using miRNeasy Mini kit (Qiagen) (3D-dermal cultures) or mRNeasy Mini kit (Qiagen) (cells) and then purified using the RNA cleanup and concentration kit (Qiagen).

Whole genome microarray analysis. The integrity of the RNA was assessed using an Agilent BioAnalyzer 2100 (Agilent Technologies). Amplification and labeling were performed with the LowInput QuickAmp Labeling Kit (Agilent Technologies). cRNAs were then hybridized on 8×60K high density SurePrint G3 human gene expression Agilent microarrays according to manufacturer's instructions (Agilent Technologies). The microarray experimental data were deposited in the NCBI GEO under the serial record number (GSE133084). The data were quantile normalized using the Bioconductor package limma. Means of ratios from all comparisons were calculated and the moderated t-statistic of the limma package provided the per gene P values. The Benjamini-Hochberg procedure was used to adjust the p-values for multiple gene comparisons.

Quantitative RT-PCR and real-time PCR. mRNA levels were determined by RT-PCR after DNase I digestion and reverse transcription using SuperScript II (Thermo Fisher Scientific). Quantitative RT-PCR were performed using the following primers: CLEC2A1 (5'-tccatcggttagcgccttg-3'/5' acagaataagtgagaaagccact-3), CLEC2A2 (5'-atgattaatccagagctgcgg-3'/5'-tctaaggggtcccagcag-3'). For quantitative real-time RT-PCR, cDNA was amplified with SYBR Green PCR Master Mix (Applied Biosystems) using a StepOne RT-PCR thermal cycler

(Applied Biosystems) following the manufacturer's instructions and data analysis was performed by ΔCT method for relative quantification. SB34 and 36B4 were both used for gene-expression data normalization. Each experimental condition was performed in triplicate. The following primers were used: CLEC2A (5′-ataccagaaattggacagcc-3′/5′-gaatgtggtgccatttgtcc-3′), KLRF2 (5′-aggcacatttactggtgattcaa-3′/5′-tgttcatctatccacatccata-3′), 36B4 (5'-tgcatcagtaccccattcta-3'/5'- aggcagatggatcagccaaga-3'), SB34 (5'-gcatcagtaccccattctatcat-3'/5'-aggtgtaatccgtctccacaga-3').

Tissue histology. 3D organotypic tissues were fixed in Antigen-Fix reagent (Diapath) for 1 h at 4°C and incubated in 34% sucrose for 16 h at 4°C prior being embedded in OCT (Tissue-Tek) and immediately frozen in liquid nitrogen. Hematoxylin and eosin staining were performed using a standard protocol on 5 µm thickness OCT sections. Skin samples were fixed in 10% neutral buffered formalin and embedded in paraffin using standard protocol.

Epidepth software. We analyzed the images with Epidepth2.1, a program dedicated to skin sample analysis. Written in Matlab (The MathWorks, Inc.) with a user-friendly interface, it automatically segments each image between the dermis, the epidermis and the invasions (in contact or not with the epidermis). Then the program automatically extracts statistical parameters to quantify the image. More specifically, we propose an "Invasion Rate" as:

$$IR = \frac{1}{L_{epi}} \sum_{j \in inv} dist_{epi}(j)$$

where $L_{epi}$is the epiderm length, $dist_{epi}(j)$ is the distance from the epiderm for all pixel "j" in an invasion. Measured in µm², this index has the advantage to take into account both the invasion sizes and how deep they migrate in the dermis. The program also manages the image library, providing statistics per experiment and per conditions. For this project we analyzed 343 images and 4390 invasions (~1s per image). Below, more details on the Epidepth (currently

version 2.1) program freely available upon request as an executable. Epidepth (currently version 2.1) is developed under Matlab fully accessible through an intuitive graphical interface.

The program will get for each image a local contrast map C:

$C(X,Y) = \frac{\sqrt{\sum_{r<r_M}\left(I(x,y)-\langle I\rangle_{d_M}(x,y)\right)^2}}{\langle I\rangle_{r_M}(x,y)}$ With $\langle I\rangle_{r_M}$ the local mean value on a disk with r_M as radius.

As a first step, the program gets automatically the contrast (tunable by user) to split the image in 3 types: background, dermis and *HC*, high contrast area, including the epidermis and invasions. In a second step, *HC* is filtered (removing too small objects) and split into the epidermis and individual invasions which can be still connected to the epidermis or not. Then the program collects parameters per invasion (area, depth from the epidermis and invasion index) and from the epidermis (area, thickness). All those parameters are sorted both per image and per category to get statistical data per condition. We also extracted the invasion index and the invasion coefficient (1) to get comparison of the methods. We chose to develop the invasion index to avoid two weaknesses of the invasion coefficient: 1) it does not depend how deep the invasion progresses in the dermis, 2) its value is highly dependent on the epidermis thickness. Even if both converge to the same conclusion, the invasion index seems to be more accurate. As mentioned, the program let to organize the data per condition. The data are summarized in graphics per image and per condition directly in the program and can be exported in Excel files to be interpreted independently. The program is available freely as an executable (thanks to the Matlab Compiler Runtime) for any user on request.

Conditioned media preparation. Cells were grown to 70% confluence, washed twice with PBS and then incubated in serum-free medium at 37°C. After 48 h, culture medium was collected, centrifuged at 300g for 5 min to remove cell debris and the supernatant stored at -80°C. Depletion of cytokines was performed by addition of 20 μg/ml of anti-IL-1α, IL-

1β or TNF-α (biolegend) 1 h at +4°C, followed by adsorption of complexes on Protein G-Sepharose 4B-beads (Sigma Aldrich) 1h at +4°C. Conditioned media was also adsorbed on Protein G-Sepharose 4B-beads as control. These conditioned media or control medium were used to stimulate fibroblasts for five days. In some experiments, 10µg/mL α-TGF-β1,2,3 neutralizing antibody (R&D) was added to SCC12_CM in the last 48 h.

Cytokine stimulations. Fibroblasts were stimulated with 2 ng/ml TGFβ1 (Peprotech), 10 ng/ml TNF-α (Peprotech), IL-1α (Peprotech) or IL-1β (R&D) for 48 h.

Flow cytometry and imaging flow cytometry. Cells were first incubated in a blocking solution to saturate Fc receptors and then incubated with 10µg/mL purified Mo anti-CLEC2A (OMA1) kindly provided Prof. Dr. Alexander Steinle (Frankfurt, Germany), purified Mo anti-MHCI W6/32, (BD Biosciences) or Mo IgG2a control isotype (BD Biosciences), followed by A488-conjugated goat anti-Mo mAb (BD Biosciences) or PE-conjugated goat anti-Mo mAb (BD Biosciences). Cells were stained with labelled-antibodies to CD90 (5E10), CD56 (B159), CD16 (3G8), NKG2D (1D11), and NKp46 (BAB281) (BD Biosciences). Fluorescence staining was analyzed on a FACScalibur (BD Biosciences) unit using CellQuest Pro Software (BD Biosciences) and FlowJo V10 software (Treestar). Imaging flow cytometry analysis were performed on an ImageStreamX MKII operated by INSPIRE software (Amnis Corporation). Cells were permeabilized using BD Cytofix/Cytoperm kit (BD Biosciences) and stained with purified Mo anti-CLEC2A (OMA1) followed by A488-conjugated goat anti-Mo (BD Biosciences). Data analysis was performed using the IDEAS software (Amnis Corporation).

Immunofluorescence staining. Cells were fixed in 3% paraformaldehyde for 20 min at RT and permeabilized with 0.5% Triton X-100 for 5 min. Following a blocking step, cells were incubated with purified Mo anti-α-SMA (Sigma Aldrich) for 1 h at RT. After washing, antibody binding was detected with A488-conjugated anti-Mo IgG secondary antibody (Thermo Fisher

Scientific). The coverslips were mounted onto glass slides using mounting media containing DAPI (Southern Biotech) and images were acquired using a Zeiss Axio Observer.Z1 fluorescent microscope.

Real-time NK cell cytotoxic assay. A real-time cytotoxic assay was performed as previously described (Fassy et al., 2017a, Fassy et al., 2017b). NK cells were isolated with the NK Cell Isolation Kit (Miltenyi Biotec). Purity was typically > 98%. NK cells were subsequently cocultured with irradiated allogeneic PBMCs and B-EBV feeder cells in X-VIVO 15 medium (Cambrex) supplemented with 10% FBS and 500 units/ml IL-2 (Chiron) to generate NK cell lines. Briefly, target cells were labelled with 0.5 µM Calcein-AM (Molecular Probes) for 15 min at room temperature. Fibroblasts F-WT3 and F-XP-C1 were additionally treated with 100 µM Indomethacin (Sigma Aldrich) to block multidrug-resistance transporters that expulse calcein. The inhibitor was maintained in the medium during the assay. Calcein-labelled targets were incubated with NK cell lines for 4 h at 37°C, 5% CO_2 and real-time monitoring of NK cell killing was performed on a Cytation™ 5 (Biotek). Cell images were processed using GEN5 software (Biotek). The percentage of lysis from triplicates was calculated as follow: % lysis = {1- [(experimental well at t/experimental well at t0)/(control well at t/control well at t0)]} x 100.

Retroviral transduction and purification. Fibroblasts were seeded at a density of 8,000 cells/cm^2 and were transduced with concentrated RV supernatants in serum-free medium for 16 h. As CD24 gene was present in the retroviral vector cassette, transduced cells were purified by flow cytometry cell sorting using FACSAria III (BD Biosciences) following staining with Mo anti-CD24-PE (Beckman Coulter) (Warrick et al., 2012).

Western blot analysis. Total proteins were extracted from fibroblasts in 8 mol/l urea buffer and protein concentrations were determined by Bradford assay (Bio-Rad). 30µg of protein for each condition were separated on 8% SDS–polyacrylamide gels and transferred onto a

polyvinyl difluoride membrane (GE Healthcare). Membranes were blocked and incubated with rabbit polyclonal anti-XPC (dilution 1/1,000; Bethyl), or anti-GAPDH (dilution 1/2,000; Abcam). After washing, membranes were stained with goat anti-rabbit HRP (1/5000; Bethyl) or rabbit anti-mouse (1/5000; Dako) HRP respectively. Blots were revealed using electrochemiluminescence reagents (GE Healthcare).

EdU incorporation. To assess EdU incorporation 2 h after 500 J/cm^2 of UVB irradiation, the the Click-iT EdU Imaging Kit (Molecular Probes) was used following the manufacturer's instructions. EdU-stained cells were mounted in standard mounting media and images were acquired a Zeiss Axio Observer.Z1 fluorescent microscope.

Statistical Analysis. Statistical analyses were performed using GraphPad Prism 8.0 software. Each statistical test is specified in the text. A *P* value <0.05 was considered as evidence for statistical significance.

References

Fassy J, Tsalkitzi K, Goncalves-Maia M, Braud VM. A Real-Time Cytotoxicity Assay as an Alternative to the Standard Chromium-51 Release Assay for Measurement of Human NK and T Cell Cytotoxic Activity. Curr Protoc Immunol 2017a;118:7 42 1-7 12.

Fassy J, Tsalkitzi K, Salavagione E, Hamouda-Tekaya N, Braud VM. A real-time digital bio-imaging system to quantify cellular cytotoxicity as an alternative to the standard chromium-51 release assay. Immunology 2017b;150:489-94.

Warrick E, Garcia M, Chagnoleau C, Chevallier O, Bergoglio V, Sartori D, et al. Preclinical corrective gene transfer in xeroderma pigmentosum human skin stem cells. Mol Ther 2012;20:798-807.